LIMNOLOGY
and
OCEANOGRAPHY: METHODS

Limnol. Oceanogr.: Methods 6, 2008, 591–609
© 2008, by the American Society of Limnology and Oceanography, Inc.

Advanced laser fluorometry of natural aquatic environments

Alexander Chekalyuk[1]* *and Mark Hafez*[2]
[1]Lamont Doherty Earth Observatory of Columbia University, Marine Biology 4a, 61 Rt. 9W, Palisades, NY 10964
[2]EG&G Services Inc., NASA Wallops Flight Facility, Bldg. N159, Wallops Island, VA

Abstract

The Advanced Laser Fluorometer (ALF) provides spectral deconvolution (SDC) analysis of the laser-stimulated emission (LSE) excited at 405 or 532 nm for assessment of chlorophyll *a*, phycoerythrin, and chromophoric dissolved organic matter. Three spectral types of phycoerythrin are discriminated for characterization of cyanobacteria and cryptophytes in mixed phototrophic populations. The SDC analysis is integrated with measurements of variable fluorescence, F_v/F_m, corrected for the SDC-retrieved background fluorescence, B_{NC}, for improved photophysiological assessments of phytoplankton. The ALF deployments in the Atlantic and Pacific Oceans, and Chesapeake, Delaware, and Monterey Bays revealed significant spectral complexity of LSE. Considerable variability in chlorophyll *a* fluorescence peak, 673-685 nm, was detected. High correlation (R^2 = 0.93) was observed in diverse water types between chlorophyll *a* concentration and fluorescence normalized to water Raman scattering. Three unidentified red bands, peaking at 625, 644, and 662 nm, were detected in the LSE excited at 405 nm. Significant variability in the B_{NC}/chlorophyll *a* ratio was observed in diverse waters. Examples of the ALF spectral correction of F_v/F_m, underway shipboard measurements of horizontal variability, and vertical distributions compiled from the discrete samples analyses are presented. The field deployments have demonstrated the utility of the ALF technique as an integrated tool for research and observations.

Introduction

Active fluorescence analysis of natural aquatic environments including oceanic, estuarine, and fresh waters is based on the measurements of the laser-induced water emission to retrieve qualitative and quantitative information about the in-situ fluorescent constituents. In vivo fluorescence of chlorophyll *a* (Chl *a*) and accessory phycobiliprotein (PBP) pigments is broadly used as an index of Chl *a* concentration and phytoplankton biomass (e.g., Falkowski and Kiefer 1985; Wirick 1994; Dandonneau and Neveux 1997) and provides useful information for structural (Yentsch and Yentsch 1979; Exton et al. 1983*b*; Yentsch and Phinney 1984, 1985; Oldham and Warner 1987; Hilton et al. 1989; Cowles et al. 1993; Poryvkina et al. 1994; Seppala and Balode 1998; Hoge et al. 1998, Beutler et al. 2002) and photophysiological (e.g., Falkowski and Kolber 1995; Kolber et al. 1998; Schreiber et al. 1993; Olson et al. 1999, 2000) characterization of the mixed algal populations. The broadband colored dissolved organic matter (CDOM) fluorescence emission can be used for assessment of CDOM abundance and its qualitative characterization (e.g., Del Castillo et al. 2000; Hudson et al. 2007).

Early studies have revealed significant spectral complexity of the actively excited emission of natural waters due to the overlap between water Raman (WR) scattering and the fluorescence bands of the aquatic constituents (Exton et al. 1983*a*,*b*; Babichenko et al. 1993; Chekalyuk et al. 1995). As pointed out by Exton et al. (1983*a*), not accounting for the spectral complexity may lead to severe problems in interpretation of the fluorescence measurements and compromise the accuracy of the fluorescence assessments. To address this issue, they proposed *(i)* to use blue and green narrow-band laser excitation to selectively stimulate the constituent fluorescence and simplify the overlapped spectral patterns, *(ii)* to conduct broadband spectral measurements of laser-stimulated emission (LSE), and *(iii)* to develop spectral deconvolution analysis of the LSE signatures to retrieve information about the aquatic fluorescent constituents

*Corresponding author: E-mail: chekaluk@ldeo.columbia.edu
Tel/Fax: 845-365-8552

Acknowledgments

This research was supported by grants from NSF (Ocean Technology and Interdisciplinary Coordination program; OCE-07-24561), NASA (Ocean Biology and Biogeochemistry program; NNX07AN44G), and NOAA/UNH (Cooperative Institute for Coastal and Estuarine Environmental Technology; NA03NOS4190195). We thank Kenneth Moore, Greg Mitchell, Mark Ohman, David Kirchman, Charles Trees, Steve Rumrill, Andrew Juhl, Jonathan Sharp, Carl Schirtzinger, Haili Wang, Brain Seegers, and Tiffany Moisan for their support of the ALF development and field measurements. Our special thanks to the anonymous reviewers for their positive critical notes and suggestions to improve the manuscript, and Roger Anderson for his kind assistance with editing.

from their overlapped spectral patterns. Some of these principles, such as multi-wavelength LSE excitation and/or broadband spectral detection, have been implemented in several shipboard and airborne laser fluorosensors (e.g., Cowles et al. 1989; Desiderio et al. 1993; Cowles et al. 1993; Babichenko et al. 1993; Chekalyuk et al. 1995; Wright et al. 2001). Nonetheless, most of the commercially available field fluorometers use spectrally broad fluorescence excitation and do not provide adequate spectral resolution to ensure reliable assessment of the fluorescent constituents in spectrally complex natural waters; no suitable spectral deconvolution algorithms have been developed to date.

In this article, we describe a new field instrument, the Advanced Laser Fluorometer (ALF), capable of fast broadband flow-through LSE spectral measurements and phytoplankton photophysiological assessments. A new analytical technique, spectral deconvolution (SDC), was developed and integrated with the ALF instrument for the real-time assessments and characterization of the key aquatic constituents, CDOM, Chl *a*, and PBP pigments, in a broad range of natural aquatic environments. In essence, the ALF/SDC analytical suite operationally implements and further advances the approach proposed by Exton et al. (1983*a*). The ALF is a portable instrument that provides underway flow-through measurements and discrete sample analysis in various shipboard and stationary settings (Fig. 1). The ALF deployments in diverse water types, including Atlantic and Pacific Oceans, and Chesapeake, Delaware, and Monterey Bays, and a number of estuaries and rivers, revealed significant spectral complexity of natural (including offshore oceanic) waters that suggests the necessity of the broadband SDC analysis. The SDC analytical technique was developed on the basis of laboratory and field measurements to retrieve from the LSE signatures the individual spectral bands of the aquatic constituents for their qualitative and quantitative assessment and spectral correction of the variable fluorescence measurements integrated with the SDC retrievals. The initial field measurements have demonstrated the utility of the ALF/SDC analytical suite as an informative integrated tool for aquatic research and bioenvironmental monitoring.

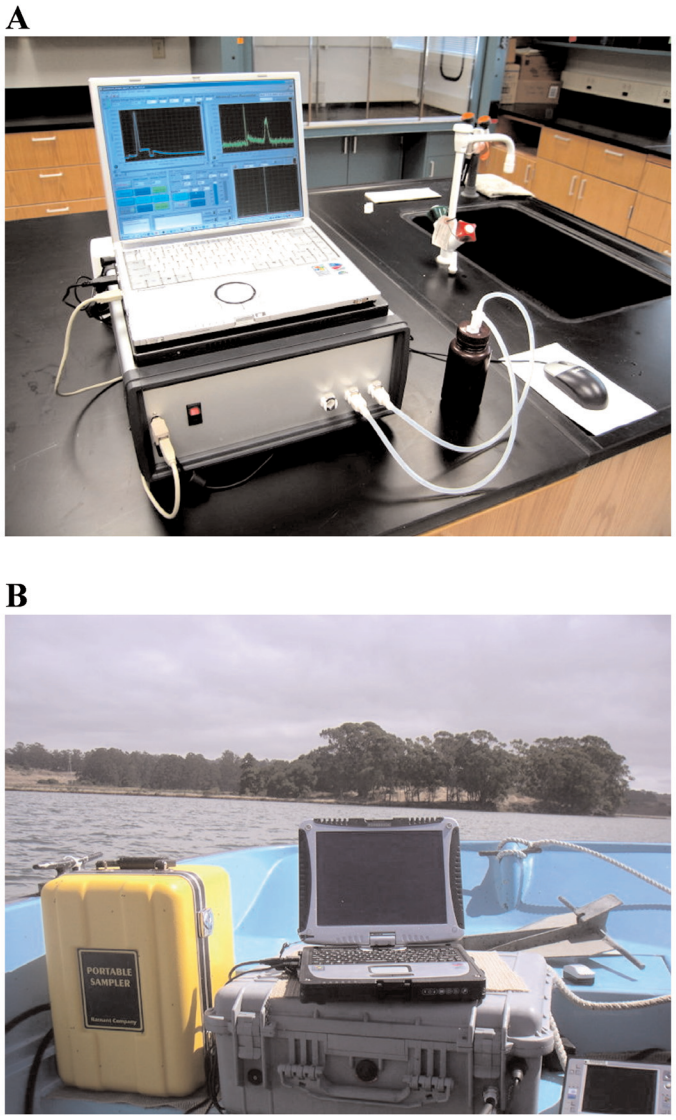

Fig. 1. The Advanced Laser Fluorometer (ALF) configured for the laboratory sample analysis (A) and for the flow-through underway measurements onboard a motorboat (B)

Materials and procedures

Advanced laser fluorometer—A diagram of the ALF instrument is presented in Fig. 2. Emission of the violet (50 mW at 405 nm; Power Technology) or green (50 mW at 532 nm; World Star Tech) lasers is alternatively directed via steering mirrors M1 and M2 in the sampled water pumped through the glass measurement cell MC (RF-1010-f, Spectrocell). The dichroic mirrors, M3 and M4 (430ASP and 505ALP, Omega Optical), reflect the laser beams back to the measurement cell to increase the signal intensity. The LSE is collected with a lens L1 (f = 25 mm; 25 mm dia.) and directed through the collimating lens and 0.6 mm optical fiber (not shown) to the input slit of the spectrometer (BTC111, B&WTek, Inc.) that measures the LSE spectrum in the 380-808 nm range (2048 pixels). The long-pass and notch filters F1 and F2 (420ALP, Omega Optical, and RNF-532.0, CVI Laser) serve to reduce laser elastic scattering in the analyzed LSE spectra. For the pump-during-probe (PDP) measurements of Chl *a* fluorescence induction, sample emission is stimulated with 200 μs PDP flashes of the 405 nm laser, which is TTL-modulated at 5 Hz repetition rate. The sample flow rate of 100 mL/min ensures assaying the low-light adapted phytoplankton cells with each of the PDP flashes. Because of present technological limitations, the 532 nm laser cannot be used for photo-physiological assessments over the single-turnover time scale (Olson et al. 1996; Kolber et al. 1998). The PDP sensor includes a lens L2 (f = 25 mm; 25 mm dia.), a band-pass interference filter F3 (685.0-10-75, Intor), a photomultiplier, PMT (H7710-02, Hamamatsu), and a 20 MHz

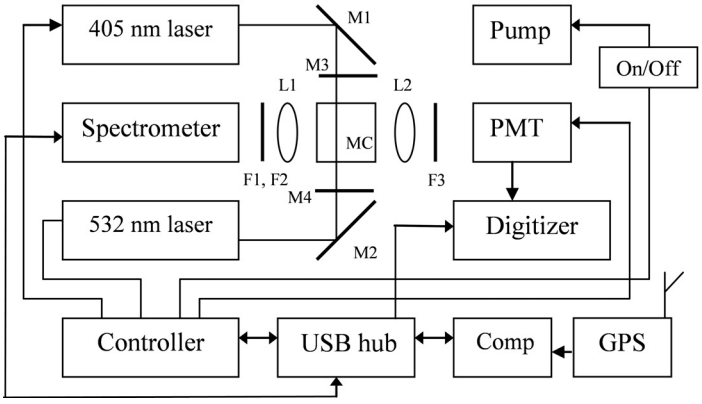

Fig. 2. Block diagram of the ALF instrument. MC – measurement cell; M3 and M4 – dichroic mirrors; F1, F2, and F3 – interference filters; L1 and L2 – lenses. See comments in the text.

12 bit waveform digitizer (3224, Pico Technology).

The ALF sampling system (Fig. 3) provides both continuous underway shipboard measurements and discrete sample analysis. Three auto-locking water connectors (PLCD16004B5, Colder Products) provide the inflow and outflow of the sampled water via the silicone tubes (Nalgene 8060-0030) (Fig. 1A). During the underway measurements, the water flow, supplied by the shipboard sampling pump, passes through the input water connector into the bottom of the measurement cell (MC). After the measurements, the water passes to the discharge connector, Out1, via a radiator (HWLabs) with a fan for heat removal from the sealed instrument case. A battery-operated peristaltic pump

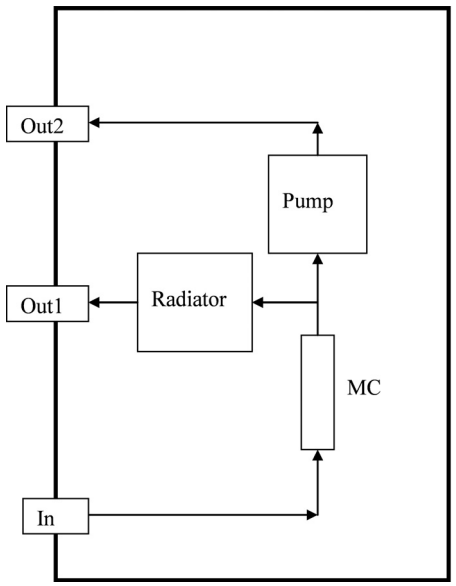

Fig. 3. Scheme of the ALF flow-through system. *Underway shipboard measurements*: the externally sampled water passes through the input connector, In, the measurement cell, MC, and the internal Radiator, to the discharge connector, Out1. *Discrete sample analysis:* the internal ALF Pump provides sample flow through In and MC to the discharge connector, Out2.

(MasterFlex 07571-00, Cole-Parmer; yellow case in Fig. 1B) is used for the ALF deployments on the small boats. The ALF instrument can also be used for flow-through monitoring at stationary settings (docks, piers, platforms, etc.), as well as for discrete sample analyses. In the latter case, a sample bottle is connected to the input water connector, In (Figs. 1, 3). The miniature diaphragm pump (NF11 KPDC, KNF Neuberger) inside the ALF instrument provides water flow through MC to the sample discharge connector, Out2. The water can be either drained to the sink or returned back to the sample bottle for sample circulation. Dark bottles of 100 – 500 mL (e.g., 141-0500, I-Chem) can be used for the measurements.

A multifunction USB board (U12, LabJack, see Fig. 2) is used to control and interface several instrument components. The lasers and the pump are controlled via digital outputs; a relay power switch (70M-ODC5, Grayhill) is also used for the pump. The PMT gain is controlled via the analog output of the board. A temperature sensor (EI1022, LabJack) is connected to the analog input to monitor the temperature inside the instrument case. A rugged notebook computer, Comp, (Toughbook, Panasonic) communicates with the controller board, the spectrograph and the digitizer via a single USB cable and a USB hub inside the ALF. A compact GPS system (76S with GA 29 antenna, Garmin) is used during the shipboard underway measurements. The 14-19 VDC power is provided by either the external AC adapter or rechargeable battery. The 160 VAH battery (PowerPad, 160 Electrovaya), enclosed with the ALF instrument in the Pelican case, can be used for 4.5 h of measurements on small boats (Fig. 1B) or in stationary settings.

An ALF operational software was developed using the LabView instrument control package (National Instruments). Each measurement cycle includes three sequent sub-cycles to measure (i) the LSE^v spectrum with 405 nm excitation, (ii) the LSE^g spectrum with 532 nm excitation, and (iii) the fluorescence induction stimulated at 405 nm. (The superscripts "v" and "g" here and below stand for the violet and green excitation, respectively). An operator can preset the LSE spectral integration time (typically, 0.3 to 3 s), the PMT gain, the duration of the PDP actinic flashes and their repetition rate, and the number of acquisitions (e.g., 5-25) to average the fluorescence induction to optimize the volume sampled during the measurement (typically, about 1 cm^3), as well as the spectral S/N ratio. The duration of the ALF measurement cycle may vary in a 5-25 s range. The measurement parameters are automatically adjusted with regard to the signal variability; the SDC and PDP data are analyzed and displayed in real time (along with the GPS data during the shipboard measurements), and stored on the computer along with the screen captures useful for documentation and data analysis. The discrete sample measurement begins with an automatic filling of the measurement cell with sampled water using the ALF pump, which is monitored via the time course of CDOM and Chl *a* fluorescence. Each sample measurement typically includes 5 to 15 measurement cycles.

Spectral deconvolution components—The SDC analyses of the ALF LSE spectral measurements is based on linear amplitude scaling of the basic spectral components to provide the best fit of the spectrum resulting from their summation to the LSE signature in the selected spectral range. A set of the SDC spectral components, {E(λ)}, was derived from the LSE spectra measured in the laboratory and field conditions and corrected for the spectrometer spectral sensitivity. The PeakFit software (SeaSolve Software, Inc.) was used for LSE spectral deconvolution to retrieve analytical approximations of the basic spectral components using the Pearson's IV function(s) to describe the asymmetrical spectral shape of the constituent emission bands:

$$y = \frac{a_0\left[1+\frac{\left(x-\frac{a_2a_4}{2a_3}-a_1\right)^2}{a_2{}^2}\right]^{-a_3}\exp\left[-a_4\left(\tan^{-1}\left(\frac{x-\frac{a_2a_4}{2a_3}-a_1}{a_2}\right)+\tan^{-1}\left(\frac{a_4}{2a_3}\right)\right)\right]}{\left(1+\frac{a_4{}^2}{4a_3{}^2}\right)^{-a_3}}$$

Here, a_0, a_1, a_2, a_3, and a_4 are parameters that define the amplitude, center, width, shape$_1$, and shape$_2$, respectively, of the Pearson's IV band.

Overall, 15 basic spectral components (Fig. 4 and Table 1) are included in the SDC procedure to account for the LSE spectral variability observed in the field. The $E_E^{v,g}$ and $E_R^{v,g}$ SDC components representing the elastic and WR scattering were retrieved from the ALF LSE measurements of twice-distilled water with analytical parameterization of their respective spectral bands using the PeakFit software. The WR scattering was approximated using several Pearson's IV components to account for its complex spectral shape. The CDOM fluorescence components were extracted from the LSE spectra of the water samples from the Delaware River that were filtered via 0.2 μm Supor filters to remove the particulate matter. The Raman and elastic scattering components were appropriately scaled and digitally subtracted from the LSE^v and LSE^g signatures of the filtrates to parameterize the residual CDOM fluorescence spectra.

A set of the LSE signatures of laboratory-grown cultures of phytoplankton and cyanobacteria was analyzed to derive several spectral components that describe spectral variability in the phycoerythrin (PE) and Chl *a* fluorescence observed in the field (see Figs. 5 and 6 and the relevant discussion in the *Assessment* for details). The cultures were provided courtesy of Dr. A. Juhl (LDEO of Columbia University); they were maintained in L1 media and diluted to concentrations close to those occurring in natural waters. The E_{C2} and E_{C3} SDC components (λ_{max} = 679 and 693 nm, respectively) were retrieved from the LSE^v spectrum of the red-tide dinoflagellate *Alexandrium Monilatum* (Juhl 2005) via digital subtraction of the CDOM background fluorescence and by a PeakFit SDC analysis and parameterization of the residual. The SDC analysis of the LSE spectra measured in the diverse water types has shown that these components can be used to describe most of the spectral variability in the 679-685 nm range, where the Chl *a* fluorescence peak is typically located. Nonetheless, several ALF field deployments during the dinoflagellate blooms have indicated significant short-wavelength shifts in the Chl *a* fluorescence peak that could be found in the 673-677 nm range (for example, see Fig. 6b and the relevant discussion in *Assessment*). The E_{C1} component (λ_{max} = 673 nm) was included in the SDC set to detect and quantify the short-wavelength Chl *a* fluorescence variability. It was derived via PeakFit parameterization of the intense short-wavelength shoulder of Chl *a* fluorescence detected in the laboratory-grown culture of dinoflagellate *Prorocentrum Scutellum* that was diluted with cold filtered seawater to induce a possible physiological response represented by the wavelength shifts.

Three additional spectral bands, E_{PE1}, E_{PE2}, and E_{PE3}, were included in the SDC set of components to address the spectral variability in the PE fluorescence (Wood et al. 1985, 1998; Ong and Glazer 1991; Lantoine and Neveux 1997; Neveux at al. 1999, 2006) that provides potential for discrimination and

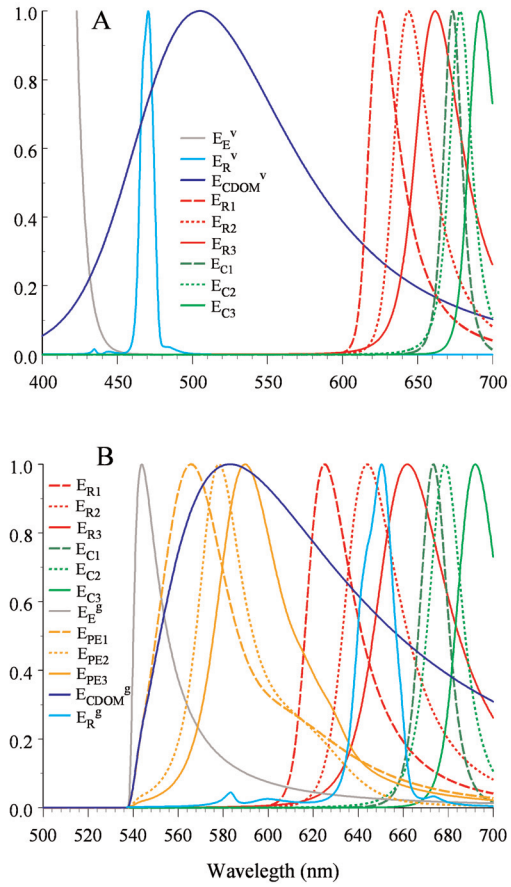

Fig. 4. The basic spectral components used for spectral deconvolution of the LSE signatures of natural waters measured with laser excitation at 405 nm (A) and 532 nm (B). See Tables 1 and 2 in Web Appendix for details. (B): The notch filter (F2 in Fig. 2) causes the cut-off at 537 nm in the elastic scattering, CDOM and PE1 fluorescence (E_E^g, E_{CDOM}^g, and E_{PE1}, respectively).

Table 1. SDC spectral components*

	Spectral component	Abbreviation	Emission peak, nm
1	Elastic scattering	E_E^v	405
2	CDOM fluorescence	E_{CDOM}^v	508
3	Water Raman scattering, 1660, 2200, and 3440 cm^{-1}	E_R^v	434, 445, 471
4	Elastic scattering	E_E^g	532
5	CDOM fluorescence	E_{CDOM}^g	587
6	Water Raman scattering, 1660, 2200, 3440 cm^{-1}	E_R^g	583, 602, 651
7	Red emission 1	E_{R1}	625
8	Red emission 2	E_{R2}	644
9	Red emission 3	E_{R3}	662
10	Chl *a* fluorescence	E_{C1}	673
11	Chl *a* fluorescence	E_{C2}	679
12	Chl *a* fluorescence	E_{C3}	693
13	PE fluorescence 1	E_{PE1}	565
14	PE fluorescence 2	E_{PE2}	578
15	PE fluorescence 3	E_{PE3}	589

*Three bands of the water Raman scattering with the Raman shifts ν_{max} = 1660, 2200, and 3440 cm^{-1}, respectively, are integrated into one SDC component representing the Raman scattering in the LSE spectra. Spectral location of the individual Raman peak can be calculated as $\lambda_{max} = (\lambda_{exc}^{-1} - \nu_{max})^{-1}$; here, λ_{max} and λ_{exc} are the wavelengths of the Raman scattering peak and excitation, respectively.

assessment of the cyanobacteria and PBP-containing eukaryotic cryptophytes in the mixed phototrophic populations (e.g., Cowles et al. 1993). In particular, the E_{PE1} SDC component (λ_{max} = 565 nm) can be used for characterization of cyanobacteria that contain the Type1 PE with high phycourobilin/phycoerythrobilin (PUB/PEB) ratio, which makes them better adapted for light harvesting in the high-transparent blue oceanic waters (Wood et al. 1998). The E_{PE2} component (λ_{max} = 578 nm) provides detection of cyanobacteria containing the low-PUB/PEB Type 2 PE that have advantage in the greenish shelf and slope waters with elevated CDOM and relatively high attenuation of blue light (Wood et al. 1998). Following the early studies (Exton et al. 1983*b*; Cowles et al. 1993; Sciandra et al. 2000), the E_{PE3} component (λ_{max} = 589 nm) was selected for assessment of PE545-containing cryptophytes (e.g., van der Weij-De Wit et al. 2006) that are often abundant in the coastal, bay and estuarine environments as shown by our recent ALF deployments. The PE SDC components were derived via the PeakFit SDC analysis of the LSE^g spectra of laboratory-grown cultures of cyanobacteria and cryptophytes containing the respective PE spectral types. In particular, the WH8102 strain of *Synechococcus sp.* (CCMP2370, Provasoli-Guillard culture collection) and unicellular PE-rich *Synechococcus*-type cyanobacteria isolated from Pensacola Bay (Juhl and Murrell 2005) were used to derive the E_{PE1} and E_{PE2} components, respectively. The fluorescence analysis of cryptophyte *Rhodomonas sp.* 768 yielded the E_{PE3} component. Along with the main maxima, the long-wavelength vibrational shoulders of the PE fluorescence (van der Weij-De Wit et al. 2006) detected by the PeakFit analysis were also included in the PE component spectra as additional Pearson's IV sub-peaks (see Table 2 in Web Appendix) to improve the SDC accuracy in the spectrally-complex yellow-red portions of the LSE^g signatures (see Fig. 6D-F).

While most of the components can be attributed to the fluorescence or scattering bands of the specific aquatic constituents, the origin of several emission bands detected in the field in the red portion of the spectrum remains to be identified (see below for details). Three spectral components, E_{R1}, E_{R2}, and E_{R3} (λ_{max} = 625, 644 and 662 nm), were included in the SDC component set to address the observed LSE variability and provide for its quantification and analysis. The spectral shape of the red SDC components was retrieved from the residual spectra composed via digital subtraction of the known overlapped SDC components from the LSE^v signatures containing the unidentified red spectral bands. The magnitudes of the Pearson's parameters, a_0, a_1, a_2, a_3 and a_4, for the spectral components used in the SDC procedure are presented in Table 2 of the Web Appendix. The peak-normalized spectral distribution for each of the components can be calculated using the Pearson's function (or a sum of the functions if several lines of Pearson's parameters are listed for the component in Table 2) with the argument $\times = \lambda$. Here, λ is the spectral wavelength in nm, e.g., 532 or 651.

SDC analysis of LSE^v spectra—The SDC processing of the LSE^v spectra involves the following steps:

1v. The measured LSE^v signature is corrected for the spectrometer spectral sensitivity and normalized to its peak to yield the $LSE^v_n(\lambda)$ signature scaled down to the normalized amplitudes of the SDC basic components to minimize the number of the SDC best-fitting iterations.

2v. $Fit^v(\lambda)$, the sum of the 9 spectral components listed in Table 1, is calculated with a set of scaling amplitude coefficients, $\{v_i\}$:

$$\begin{aligned} Fit^v(\lambda) = {} & v_1 E_R^v(\lambda) + v_2 E_E^v(\lambda) + v_3 E_{CDOM}^v(\lambda) + \\ & v_4 E_{C1}(\lambda) + v_5 E_{C2}(\lambda) + v_6 E_{C3}(\lambda) + \\ & v_7 E_{R1}(\lambda) + v_8 E_{R2}(\lambda) + v_9 E_{R3}(\lambda) \end{aligned} \quad (1)$$

Here, λ is a spectral wavelength. The magnitudes of the scaling coefficients are varied until the sum of squares of residuals between the Fit^v and LSE^v_n is minimized in the fitting spectral range (e.g., Nash 1979). For the ALF LSE^v measurements, the fitting range includes two spectral sub-ranges, 423 to 515 nm, and 550 to 700 nm, where the emission peaks of the key aquatic constituents are located in the LSE^v spectra (see Fig. 5). The initial (380-423 nm) and intermediate green (515-550 nm) portions of the LSE^v signatures, where F1 and F2 filters of the ALF spectrometer have high optical density, are excluded from the SDC analysis. The NIR portion (700-808 nm) is also excluded because of the NIR decline in the spectrometer sensitivity.

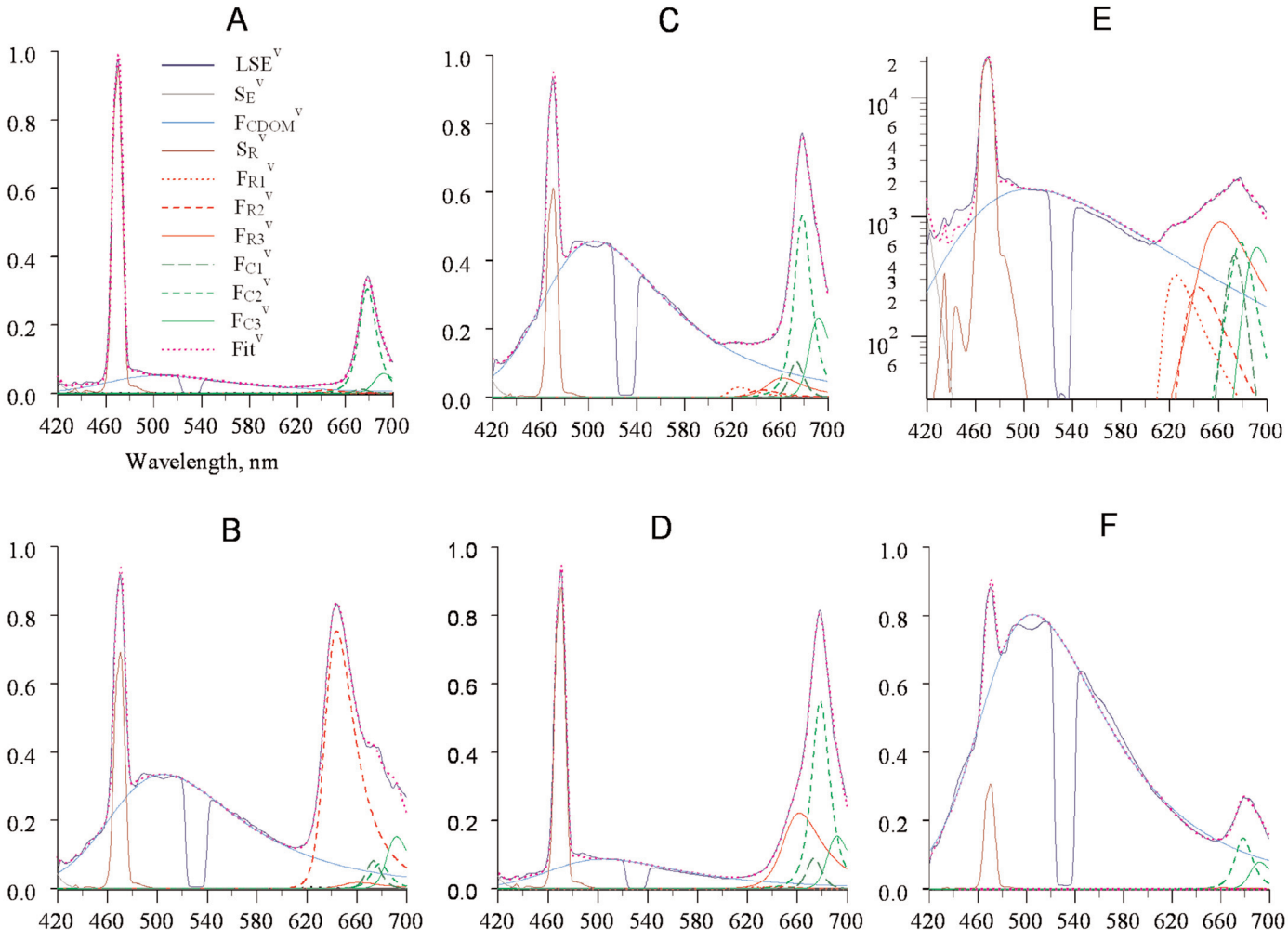

Fig. 5. Variability in the LSE^v spectra measured in diverse water types with laser excitation at 405 nm. (A): Surface sample, Southern California Bight, April 2007. Surface sampling in lower Delaware Bay, March 2006 (B) and April 2006 (C). (D): Underway measurements in the Southern California Bight, April 2007. (E): Sample from 100 m depth taken at the same location as (A). (F): Surface sample, Delaware River, June 2006. The cut-off in the LSE^v around 532 nm was caused by the notch filter (F2 in Fig. 2).

3v. The retrieved values of scaling coefficients are used to calculate the SDC components of the LSE^v_n signature that are displayed by the ALF software in the LSE^v spectral panel along with the LSE^v_n and Fit^v spectra to visualize the results of best fitting (for example, see Fig. 5):

$$\begin{aligned} S_R^v(\lambda) &= v_1 E_R^v(\lambda) \\ S_E^v(\lambda) &= v_2 E_E^v(\lambda) \\ F_{CDOM}^v(\lambda) &= v_3 E_{CDOM}^v(\lambda) \\ F_{C1}^v(\lambda) &= v_4 E_{C1}(\lambda) \\ F_{C2}^v(\lambda) &= v_5 E_{C2}(\lambda) \\ F_{C3}^v(\lambda) &= v_6 E_{C3}(\lambda) \\ F_{R1}^v(\lambda) &= v_7 E_{R1}(\lambda) \\ F_{R2}^v(\lambda) &= v_8 E_{R3}(\lambda) \\ F_{R3}^v(\lambda) &= v_9 E_{R3}(\lambda) \end{aligned} \qquad (2)$$

In addition, the SDC ALF algorithm integrates the F_{C1}^v, F_{C2}^v, and F_{C3}^v spectral components to synthesize the Chl *a* fluorescence component of the LSE^v_n spectrum:

$$\begin{aligned} F_{Chla}^v(\lambda) &= v_4 E_{C1}(\lambda) + v_5 E_{C2}(\lambda) + v_6 E_{C3}(\lambda) \\ v_{Chla} &= \max[F_{Chla}^v(\lambda)] \end{aligned} \qquad (3)$$

Here, v_{Chla} is the $F_{Chla}^v(\lambda)$ peak magnitude. The $F_{Chla}^v(\lambda)$ synthesis permits accounting for the spectral variability in Chl *a* fluorescence observed in the field (for details, see Fig. 5 and relevant discussion in *Assessment*). The wavelength of the $F_{Chla}^v(\lambda)$ peak, λ_{Chla}^v, is also determined for assessment of the spectral variability in Chl *a* fluorescence and spectral correction of variable fluorescence as described below.

4v. A set of relative parameters for the LSE^v spectral components is calculated as

$$\begin{aligned} I_{Chla/R}{}^{v} &= v_{Chla} v_1^{-1} \\ I_{CDOM/R}{}^{v} &= v_3 v_1^{-1} \\ I_{R1/R}{}^{v} &= v_7 v_1^{-1} \\ I_{R2/R}{}^{v} &= v_8 v_1^{-1} \\ I_{R3/R}{}^{v} &= v_9 v_1^{-1} \end{aligned} \quad (4)$$

These parameters represent normalized to WR^v signal intensities of the constituent fluorescence bands contributing to the LSE^v spectrum. They are used for quantitative assessment of the major fluorescence constituents, such as Chl *a* or CDOM (Klyshko and Fadeev 1978; Hoge and Swift 1981; Babichenko et al. 1993; Chekalyuk et al. 1995; see Fig. 7 for example) and for parameterization of the LSE^v spectral shape, which can be described with the set of five relative parameters determined by Eq. 4.

SDC analysis of LSE^g spectra—The SDC analysis of the LSE^g spectra is basically similar to the LSE^v SDC analysis, though three additional components are included in the SDC procedure to account for the spectral variability in PE fluorescence (e.g., Cowles et al. 1993) efficiently stimulated with the green laser excitation. The SDC processing of the LSE^g spectra includes the following steps:

1g. The LSE^g spectrum measured by the ALF instrument is corrected for the instrument spectral sensitivity and normalized to its peak to yield the $LSE^g{}_n(\lambda)$ signature.

2g. $Fit^g(\lambda)$, the sum of the 12 spectral components listed in Table 1, is calculated with a set of scaling coefficients $\{g_i\}$:

$$\begin{aligned} Fit^g(\lambda) = {} & g_1 E_R{}^g(\lambda) + g_2 E_E{}^g(\lambda) + g_3 E_{CDOM}{}^g(\lambda) + \\ & g_4 E_{C1}(\lambda) + g_5 E_{C2}(\lambda) + g_6 E_{C3}(\lambda) + \\ & g_7 E_{R1}(\lambda) + g_8 E_{R2}(\lambda) + g_9 E_{R3}(\lambda) + \\ & g_{10} E_{PE1}(\lambda) + g_{11} E_{PE2}(\lambda) + g_{12} E_{PE3}(\lambda) \end{aligned} \quad (5)$$

Magnitudes of the scaling coefficients are varied until the sum of squares of residuals between the Fit^g and $LSE^g{}_n$ is minimized in the spectral range of SDC fitting, 544 to 700 nm, where the emission peaks of the key aquatic constituents are located in the LSE^g spectra (see Fig. 6).

3g. The retrieved $\{g_i\}$ values are then used to calculate the SDC components of the $LSE^g{}_n$ signature to visualize the results of best fitting (for example, see Fig. 6):

$$\begin{aligned} S_R{}^g(\lambda) &= g_1 E_R{}^g(\lambda) \\ S_E{}^g(\lambda) &= g_2 S_E{}^g(\lambda) \\ F_{CDOM}{}^g(\lambda) &= g_3 E_{CDOM}{}^g(\lambda) \\ F_{C1}{}^g(\lambda) &= g_4 E_{C1}(\lambda) \\ F_{C2}{}^g(\lambda) &= g_5 E_{C2}(\lambda) \\ F_{C3}{}^g(\lambda) &= g_6 E_{C3}(\lambda) \\ F_{R1}{}^g(\lambda) &= g_7 E_{R1}(\lambda) \\ F_{R2}{}^g(\lambda) &= g_8 E_{R3}(\lambda) \\ F_{R3}{}^g(\lambda) &= g_9 E_{R3}(\lambda) \\ F_{PE1}{}^g(\lambda) &= g_{10} E_{PE1}(\lambda) \\ F_{PE2}{}^g(\lambda) &= g_{11} E_{PE2}(\lambda) \\ F_{PE3}{}^g(\lambda) &= g_{12} E_{PE3}(\lambda) \end{aligned} \quad (6)$$

Similar to the SDC analysis of the LSE^v spectra, the $F_{C1}{}^g(\lambda)$, $F_{C2}{}^g(\lambda)$, and $F_{C3}{}^g(\lambda)$ spectra are used to synthesize $F_{Chla}{}^g(\lambda)$, the Chl *a* fluorescence component of the $LSE^g{}_n$ spectrum, and determine the $F_{Chla}{}^g(\lambda)$ peak magnitude, g_{Chla}:

$$\begin{aligned} F_{Chla}{}^g(\lambda) &= g_4 E_{C1}(\lambda) + g_5 E_{C2}(\lambda) + g_6 E_{C3}(\lambda) \\ g_{Chla} &= \max[F_{Chla}{}^g(\lambda)] \end{aligned} \quad (7)$$

The wavelength of the $F_{Chla}{}^g(\lambda)$ peak, $\lambda_{Chla}{}^g$, is also determined for assessment of the spectral variability in Chl *a* fluorescence.

The SDC retrievals of the $F_{PE1}{}^g(\lambda)$ and $F_{PE2}{}^g(\lambda)$ bands can be used for discrimination and assessment of the Type 1 and Type 2 PE-containing cyanobacteria, respectively. In addition, the integrated synthetic cyanobacterial PE fluorescence band, $F_{PE12}{}^g(\lambda)$, and its peak magnitude, g_{PE12}, are also generated for the overall assessment of the PE-containing cyanobacterial population:

$$\begin{aligned} F_{PE12}{}^g(\lambda) &= g_{10} E_{PE1}(\lambda) + g_{11} E_{PE2}(\lambda) \\ g_{PE12} &= \max[F_{PE12}{}^g(\lambda)] \end{aligned} \quad (8)$$

These parameters can be used to examine their relationship with high-performance liquid chromatography (HPLC) and other analyses that do not discriminate within the cyanobacterial group.

4g. A set of relative parameters for the LSE^g spectral components is calculated as

$$\begin{aligned} I_{Chla/R}{}^g(\lambda) &= g_{Chla} g_1^{-1} \\ I_{CDOM/R}{}^g &= g_3\, g_1^{-1} \\ I_{R1/R}{}^g &= g_7\, g_1^{-1} \\ I_{R2/R}{}^g &= g_8\, g_1^{-1} \\ I_{R3/R}{}^g &= g_9\, g_1^{-1} \\ I_{PE1/R}{}^g &= g_{10}\, g_1^{-1} \\ I_{PE2/R}{}^g &= g_{11}\, g_1^{-1} \\ I_{PE3/R}{}^g &= g_{12}\, g_1^{-1} \end{aligned} \quad (9)$$

These parameters represent WR^g-normalized peak intensities of the major fluorescence bands contributing to formation of the LSE^g signature. As analogue parameters retrieved from the LSE^v SDC analysis, they can be used for quantitative assessment of the major fluorescence constituents, such as Chl *a*, PE, or CDOM and for parameterization of the LSE^g spectral shape, which can be described with the set of eight relative parameters determined by Eq. 9. Several additional parameters, which may provide useful indexes for structural characterization of the mixed population of phytoplankton and cyanobacteria (e.g., Fig. 8), are also calculated:

$$\begin{aligned} I_{PE12/Chla} &= g_{PE12}\, g_{Chl}^{-1} \\ I_{PE1/Chla} &= g_{10}\, g_{Chl}^{-1} \\ I_{PE2/Chla} &= g_{11}\, g_{Chl}^{-1} \\ I_{PE3/Chla} &= g_{12}\, g_{Chl}^{-1} \\ I_{PE1/PE2} &= g_{10}\, g_{11}^{-1} \end{aligned} \quad (10)$$

Spectral correction of variable fluorescence—The Chl *a* fluorescence induction, caused by the gradual closure of the reaction centers of photosystem II (PSII), occur over the single PSII turnover time scale (i.e., 40-100 μs) with the appropriate excitation flux (Kolber et al. 1998; Olson et al. 1996). The parameters

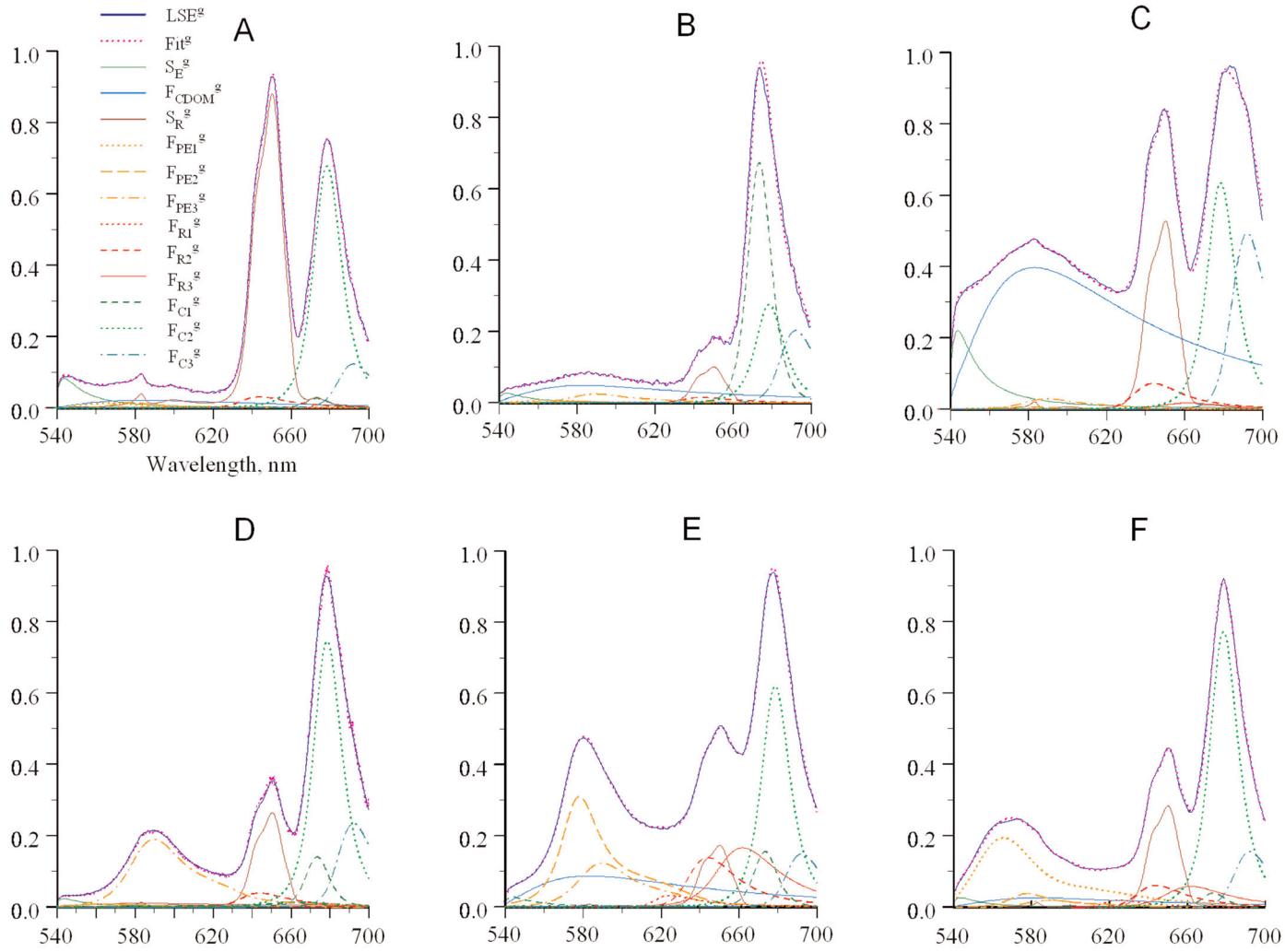

Fig. 6. Variability in the LSE^g spectra measured in diverse surface waters with excitation at 532 nm. (A): Southern California Bight, April 2007. (B): Moss Landing Harbor (California), September 2006. (C): Delaware River, June 2006. (D): Coastal zone of the Southern California Bight near Point Conception, April 2007. (E): Lower Chesapeake Bay, June 2005. (F): Middle Atlantic Bight, vicinity of the Delaware Bay mouth, June 2006.

of variable fluorescence, a proxy of the quantum yield of PSII photochemistry and handy index of photo-physiological status of photosynthesizing organisms (e.g., Falkowski and Kolber 1995), can be retrieved from the PDP induction measurements as described by Olson et al. (1996). In particular, the Chl *a* fluorescence induction, $F_{Chla}(t)$, measured using the PDP excitation protocol employed in the ALF instrument can be approximated (Olson et al. 1996) as:

$$F_{Chla}(t) = [F_m^{-1} - (F_m^{-1} - F_o^{-1}) \exp(-t/A)]^{-1} \quad (11)$$

Here, F_o and F_m are the initial and maximum intensity of Chl *a* fluorescence; A is a time constant. The nonlinear best fitting with Eq. 11 to the measured Chl *a* fluorescence induction yields the parameters of variable fluorescence, F_o, F_m, and A. The magnitude of variable fluorescence can be calculated as $F_v/F_m = (F_m - F_o)/F_m$.

As pointed out by Cullen and Davis (2003), the fluorescence induction measured in natural waters often needs to be corrected for the non-Chl *a* background emission, B_{NC}, produced by the broadband CDOM fluorescence in the area of the Chl *a* fluorescence peak (e.g., Fig. 5F). Elevated levels of phaeophytin may also affect measurements of the variable fluorescence (Fuchs et al. 2002). Other constituents present in natural waters may also contribute to the B_{NC} in this spectral region (for example, see Fig. 5B, 5C, 5E, and 5D). The B_{NC} magnitude remains unchanged during the Chl *a* fluorescence induction, as it has no relation to the dynamic changes in the PSII status stimulated by the actinic flash. Not accounting for the B_{NC} background may result in flattening the induction curves and underestimating the variable fluorescence, which may be significant even in the offshore oceanic waters with low CDOM content (Laney and Letelier 2008).

Most fluorometers that measure variable fluorescence do not possess adequate spectral resolution for discrimination between the Chl *a* fluorescence and B_{NC}. Cullen and Davis (2003) proposed periodical measurements of the blanks and filtrates to address the issue. Laney and Letelier (2008) have further advanced this approach via automatic assaying the filtrate fluorescence each hour during the continuous underway flow-through measurements. Though it may partially improve the F_v/F_m assessments, the variable fluorescence retrievals need to be corrected for the B_{NC} background measured in the same water sample to account for the B_{NC} spatial and temporal variability. Also, both dissolved and particulate (e.g., Fuchs et al. 2002) organic matter present in natural waters may contribute to the B_{NC} background, while the filtrate measurements account only for the dissolved component.

The ALF instrument, which uniquely combines both spectrally and temporally resolved LSE measurements of the sampled water, provides potential for retrieving from the induction measurements the actual Chl *a* fluorescence signal and its spectral discrimination regardless of the B_{NC} origin and magnitude. Because the induction and spectral measurements are conducted in continuous flow of the sampled water with a few seconds delay, the spectrally and temporally resolved measurements represent the same analyzed water and can be directly related. The intensity of non-Chl *a* fluorescence background in the LSE^v_n spectrum can be assessed via subtracting the SDC-retrieved spectral peak magnitude of the Chl *a* fluorescence, v_{Chla} (see Eq.3), from the LSE^v_n spectral intensity around Chl *a* peak, $LSE^v_n(\lambda_{Chla}{}^v)$. The $I_{NC/Chla}$ parameter to assess the ratio of the non-Chl *a* background to the v_{Chla} magnitude can be therefore calculated from the SDC LSE^v analysis as:

$$I_{NC/Chla} = LSE^v_n(\lambda_{Chla}{}^v)\ v_{Chla}{}^{-1} - 1 \qquad (12)$$

The $I_{NC/Chla}$ spectral retrievals can be used for correction of the PDP measurements of fluorescence induction for the non-Chl *a* background emission to improve phytoplankton photophysiological assessments of variable fluorescence. The relationship between the $I_{NC/Chla}$ parameter yielded by the SDC analysis of the LSE spectrum and the B_{NC} magnitude in the fluorescence induction is not trivial. The intensity of the 405 nm laser excitation is the same for measuring both the LSE^v spectra and PDP fluorescence induction. Therefore, during the LSE^v spectral acquisition (1-3 s), the Chl *a* fluorescence exhibits the initial fast (~ 50 μs) PDP induction rise followed by several additional transitional stages known as Kautsky effect (e.g., Govindjee 1995; Lazar 1999) to reach the steady-state level approximately equal to its initial magnitude when the excitation is turned on. Therefore the $I_{NC/Chla}$ value derived from the SDC LSE analysis is determined by the average over the spectral acquisition time magnitude of the Chl *a* fluorescence yield. The latter is close to the mean magnitude of the Chl *a* yield during the PDP induction measurements under conditions of the ALF measurements. Thus, to a first approximation, the B_{NC} background and the B_{NC}-corrected time course of variable fluorescence, $F_{Chla}(t)$, can be estimated as (see Fig. 9B for illustration):

$$B_{NC} = (1 + I_{NC/Chla}{}^{-1})^{-1}\ \text{mean}(F_{PDP}(t)), \text{ and} \qquad (13)$$

$$F_{Chla}(t) = F_{PDP}(t) - B_{NC}. \qquad (14)$$

Here $F_{PDP}(t)$ is the time course of PDP fluorescence induction measured by the ALF instrument. Eqs. 13 and 14 are used during the real-time processing of the ALF PDP measurements to retrieve $F_{Chla}(t)$. The non-linear fitting with Eq. 11 provides then the B_{NC}-corrected magnitude of variable fluorescence, $F_v/F_m = (F_m\text{-}F_o)/F_m$. For evaluation, the non-spectrally corrected magnitude of variable fluorescence, $F_v/F_m{}^{NC}$, is also calculated from results of fitting with Eq. 11 to $F_{PDP}(t)$.

Assessment

LSE^v spectral variability—Development of the SDC analytical algorithms introduced in *Materials and Procedures* to a large extent built upon a series of ALF field deployments conducted in 2005-2007. The objectives were (i) to test the ALF instrument in a broad range of natural aquatic environments and (ii) to develop a simple yet adequate SDC procedure that would provide accurate retrievals of the constituent emission bands from the complex overlapped LSE spectral patterns. Regionally, the ALF deployments included the offshore and coastal zones of the Atlantic and Pacific Oceans, and Chesapeake, Delaware and Monterey Bays, and a number of estuaries and rivers of the East and West US coast.

Some examples of the LSE^v spectral variability observed during the field measurements are presented in Fig. 5 along with the SDC analyses of the LSE^v signatures. The blue solid and the light magenta dotted lines display the measured spectra and the SDC best fits, respectively. As evident from Fig. 5, in most cases, the SDC fits are almost indistinguishable from the measured spectra except some minor deviations around the CDOM fluorescence peak. The LSE^v signatures measured in the surface off-shore oceanic waters were relatively simple and mostly determined by the overlapped bands of the WR scattering ($S_R{}^v$), broadband CDOM fluorescence ($F_{CDOM}{}^v$), and Chl *a* fluorescence ($F_{C2}{}^v$, $F_{C3}{}^v$) (for example, Fig. 5A; Southern California Bight, April 2007). Up to two orders of magnitude of variability in the $F_{CDOM}{}^v$ intensity relative to the $S_R{}^v$ peak were observed due to significant variations in the CDOM content in different water types. For example, compare the LSE^v spectra measured in oceanic waters (Fig.5A), Delaware Bay (Fig.5B), and Delaware River (Fig.5F). The $E_{CDOM}{}^v$ component, derived from the ALF measurements in the Delaware River, was found to work well in all measured water types, including the offshore oceanic waters, despite the known chemical and spectral complexity and variability of CDOM in natural waters (e.g., Del Castillo et al. 2000; Hudson et al. 2007, and references therein). We hypothesize that the satisfactory SDC performance of the simple single CDOM component, $E_{CDOM}{}^v$, may be

due to the relatively long-wavelength excitation, 405 nm, used in the ALF instrument. Chl *a* fluorescence was a major contributor to the LSE^v in the red portion of the spectra. Though the $F_{Chla}{}^v$ peak was located around 680 nm in most of the LSE^v signatures, both blue and red shifts in the peak location, ca. 677 to 685 nm, accompanied by changes in its spectral shape were detected. Most of the spectral variability in the Chl *a* fluorescence was reasonably well described via linear scaling the E_{C1}, E_{C2}, and E_{C3} SDC components (see Eq. 3).

Along with the Chl *a* fluorescence, three other spectrally distinct emission bands were detected in the red portion of the LSE^v spectra during the ALF field deployments. The underway ALF measurements in the Delaware Bay in March 2006 revealed an intense emission peak at 644 nm that significantly exceeded the Chl *a* fluorescence (Fig. 5B). Similar though less extreme spectral patterns were also observed during the underway measurements in the coastal zone of the Middle-Atlantic Bight near the Chincoteague Island in March 2006. Another spectral band with maximum around 625 nm was detected during the ALF underway measurements in the surface waters of the Delaware Bay in April 2006 (Fig. 5C). The emission band peaking at 662 nm was observed in the LSE^v signatures at various locations during the ALF underway measurements (for example, see Fig. 5D). Finally, the broadband red emission ranging from 610 to 700 nm, which seemed to be composed of several overlapped emission bands, was consistently detected in the LSE^v spectra of the water samples taken in the euphotic layer below the Chl *a* maximum in the Southern California Bight, California Current and in the Middle Atlantic Bight (for example, Fig. 5E). The E_{R1}, E_{R2}, and E_{R3} SDC spectral component were derived from the LSE^v field data (see above) to account for the observed variability in the red portion of the LSE^v signatures. As evident from Fig. 5, they describe well not only the individual spectral bands detected in the surface waters (panels B, C, and D), but also the broadband red emission observed in the water samples taken from the bottom of the euphotic layer (panel E).

The origin of the red emission bands peaking at 625, 644, and 662 nm in the LSE^v spectra stimulated to 405 nm remains to be identified. Based on their spectral location and characteristic shape, they might be interpreted as fluorescence of PBP pigments. Indeed, the cryptophyte-specific phycoerythrin PE566 has an in vivo emission peak around 620 nm (Mimuro et al.1998). The fluorescence maximum of phycocyanin, an accessory PBP pigment present in cyanobacteria and cryptophytes, is located in the 642-645 nm range, while some spectral forms of cyanobacterial allophycocyanin have their emission peaks around 662 nm (e.g., Heocha 1965; Wood et al. 1985). Despite the spectral similarity, the PBP origin of the red fluorescence in the LSE^v spectra seems be doubtful. Indeed, the SDC analysis of the LSE^g signatures has detected no respective red fluorescence, though the green excitation is known to be more efficient than the violet one in stimulating the in vivo PBP emission. Also, no significant correlation was found between the red emission detected in the LSE^v spectra and the PE fluorescence observed in the LSE^g signatures. We hypothesize that the red emission detected in some LSE^v signatures might rather originate from a dysfunctional or degrading photosynthetic apparatus of phytoplankton. In particular, the 644 nm emission peak could be attributed to the accessory chlorophyll c (Chl-c) from poorly-functional light-harvesting complexes. The weak in vivo Chl *c* fluorescence peaking at 644 nm was reported from photosynthetically functional phytoplankton (e.g., van der Weij-De Wit et al. 2006). Regarding the emission at 662 nm, similar spectral features can be observed in the LSE^{405} signatures of senescent phytoplankton cultures, consistently with the presumable photodegradation origin of the emission. Additional investigations need to be conducted to identify the red emission bands observed in the field.

LSE^g spectral variability—Some characteristic spectral features of the LSE^g signatures of natural waters are illustrated in Fig. 6. Despite their significant variability, the SDC best fits (dotted light magenta) well reproduce the measured LSE^g spectra (blue solid lines). The WR scattering band, $S_R{}^g$, has its major maximum at 651 nm (the Raman shift ν_{max} = 3440 cm^{-1}) and is a dominant or subdominant spectral component in most of the LSE^g spectra. Two less intense WR bands, 1600 and 2200 cm^{-1}, also can be seen in the LSE^g spectra at 583 and 602 nm in Fig. 6A. Although their intensities are only a few percent of the major Raman peak at 651 nm, they play important role in formation of the LSE^g patterns in the oceanic waters, where CDOM and PE fluorescence are often comparable to the intensity of these weak Raman bands (Fig. 6A).

As evident from Fig. 6, Chl *a* fluorescence is another important contributor to the LSE^g spectra of natural waters. Significant variability in the location (673-686 nm) and spectral shape of the Chl *a* fluorescence band was observed during the ALF field measurements. For example, a short-wavelength spectral shift in the Chl *a* fluorescence was detected during the dinoflagellate blooms in Monterey Bay and adjacent Elkhorn Slough in September 2006 (for example, Fig. 6B, $\lambda_{Chla}{}^g$ = 673 nm), in the lower Chesapeake Bay and adjacent York River in July 2005 (e.g., Fig. 6E, $\lambda_{Chla}{}^g$ = 676 nm), and in the Pacific coastal zone of San Diego in June 2005 ($\lambda_{Chla}{}^g$ = 675 nm). High linear anti-correlation (R^2 = 0.90) between the blue shift and decline in variable fluorescence observed in the Monterey Bay suggests a potential physiological origin of the spectral shift. For instance, the dinoflagellate-specific water soluble peridinin-chlorophyll-protein light-harvesting complexes (sPCP LHC) do not fluoresce in the normally functional PSII, but are known to have their sPCP-specific Chl *a* fluorescence peak around 673-676 nm (Iglesias-Prieto et al. 1991). A decrease in the efficiency of energy transfer from the sPCP LHC to the PSII core might lead to appearance of the sPCP Chl *a* fluorescence accompanied by decline in Chl *a* fluorescence from the core, which could result in the blue shift of the overall Chl *a* peak. The fact that the blue shift was stronger with the green vs. violet excitation is consistent with such an assumption, because the peridinin absorption peak locates in the green spectral region.

The red spectral shifts in Chl *a* fluorescence were also observed during the ALF field deployments. For example, the Chl *a* emission peaking at 686 nm with the shoulder at 692 nm was detected in both LSE^v and LSE^g spectra measured in the Delaware River (for example, Figs. 5F and 6C). As evident from the SDC examples presented in Figs 5 and 6, the observed field-based spectral variability in Chl *a* fluorescence can be reasonably well described via SDC linear scaling of the E_{C1}, E_{C2}, and E_{C3} spectral components. The acquired field data will be reported and analyzed in more detail in a series of follow-up publications. The origin of the spectral variability, which may be driven by both structural and physiological changes in the algae, will be further investigated in subsequent stages of the ALF/SDC research.

A distinct feature of the LSE^g signatures is the significant variability in the 540-620 nm portions of the spectra mainly caused by the overlap of the PE and CDOM fluorescence bands (Fig. 6). The ALF/SDC analyses often detected significant cryptophyte-specific fluorescence, $F_{PE3}{}^g$ (λ_{max} = 589 nm), in this spectral range of the LSE^g spectra measured in various coastal, estuarine and fresh waters examined. For example, see Fig. 6D and 6E measured respectively near Point Conception in the Southern California Bight (April 2007; similar patterns were observed in May 2006) and in the lower Chesapeake Bay (July 2005). The significant $F_{PE3}{}^g$ fluorescence was also detected in the upper and middle portions of the Delaware Bay in June 2006, in the York River (Virginia) in July 2005, and in the Sough Slough estuary (Oregon) in April 2005. The cyanobacterial high PUB/PEB (Type 1) PE fluorescence, $F_{PE1}{}^g$ (λ_{max} = 565 nm), dominated in the yellow-orange LSE^g region in the samples obtained in the zone of Middle Atlantic Bight adjacent to the Delaware Bay (Fig. 6F, June 2006); similarly significant though less intense $F_{PE1}{}^g$ fluorescence was consistently detected in the offshore waters of the Middle Atlantic Bight (see a transect distribution of $I_{PE1/R}{}^g$ in Fig. 10) and in the California current in May 2006 and April 2007. Fluorescence of low PUB/PEB, Type 2 spectral form of cyanobacterial PE, $F_{PE2}{}^g$ (λ_{max} = 578 nm), was found to often accompany the $F_{PE1}{}^g$ and/or $F_{PE3}{}^g$ emission in coastal, bay, and estuarine environments (for example, Figs. 6E and 6F). It dominated in the LSE^g spectra between 540 and 620 nm in the lower Chesapeake Bay (Fig. 6E, July 2005) and coastal waters of Hawaii Island (February 2006); the significant $F_{PE2}{}^g$ emission was also found in the LSE^g spectra measured in the lower Delaware Bay in June 2005 and near-shore Pacific zone of California (May 2006 and April 2007).

The broadband CDOM emission, $F_{CDOM}{}^g$, though less intense vs. the WR band as compared with the LSE^v signatures, still played an important role in the formation of the orange-red portion of the LSE^g spectra not only in estuaries, as pointed out by Exton et al. (1983*a*), but in all the surveyed water types, including offshore oceanic waters. Its intensity was often comparable with PE fluorescence in the bay and estuarine waters (e.g., Fig. 6E) and could dominate over the PE emission peaks in both oceanic (Fig. 6A) and fresh waters. For example, in the Delaware River (Fig. 6C, June 2006), about 85% of the LSE^{532} intensity in the 570-620 nm range, which is often interpreted as the PE fluorescence, was actually formed by the CDOM emission (confirmed by the spectral measurement of the sample filtrates). In the CDOM-rich waters, the intense CDOM fluorescence may provide significant background contributions even in the red portion of the LSE^g spectra that needs to be accounted for correct assessment of the red emission bands, such as WR scattering or Chl *a* fluorescence (Fig. 6C, 6E).

The SDC analysis of the LSE^g field measurements has revealed that the linear scaling of the SDC spectral components, attributed to the WR scattering and fluorescence of Chl *a*, PE, and CDOM, cannot entirely account for the complex spectral patterns observed in the red portion of the LSE^g spectra. The SDC mismatch was particularly evident for the LSE^g signatures that showed the intense PE fluorescence, thus indicating significant abundance of PBP-containing cryptophytes and/or cyanobacteria. For evaluation, three additional spectral components, E_{R1}, E_{R2}, and E_{R3}, which were originally derived from the LSE^v field data, were included in the SDC procedure described by Eq. 5. This was done to incorporate in the best fitting three additional red spectral bands, $F_{R1}{}^g$, $F_{R2}{}^g$, and $F_{R3}{}^g$ (see Eq. 6). The SDC analysis has shown that the $F_{R1}{}^g$ band played a rather insignificant role in the LSE^g formation for most of the explored water types; while the $F_{R2}{}^g$ and $F_{R3}{}^g$ SDC spectral components provided variable contributions in various waters, remaining subdominant relative to the major peaks of WR scattering at 651 nm, Chl *a*, and PE fluorescence (for example, see Fig. 6). The LSE^g patterns observed in the lower Chesapeake Bay in June 2005 (i.e., Fig. 6E) constituted an exception, as all three red emission bands provided significant contributions to the LSE^g formation, comparable to the usually dominant band of WR scattering, $S_R{}^g$. The correlation patterns with the group-specific spectral types of PE emission suggest that in the areas abundant with PBP-containing cyanobacteria and cryptophytes the $F_{R2}{}^g$ and $F_{R3}{}^g$ SDC retrievals may be associated with the phycocyanin and allophycocyanin fluorescence.

Correlation analysis of the SDC retrievals—To evaluate ALF capacity for quantitative assessments of aquatic fluorescent constituents, the ALF spectral retrievals were compared with HPLC pigment analyses. The $I_{Chla/R}{}^v$ and $I_{Chla/R}{}^g$ SDC retrievals (see Eqs. 4 and 9) showed high correlation with the HPLC assessments of Chl *a* concentration in a range of water types surveyed during the ALF field deployments. For example, Fig. 7A displays the linear correlation (R^2 = 0.93) between the $I_{Chla/R}{}^v$ retrievals and the HPLC measurements of total Chl *a* conducted in the Middle Atlantic Bight, Chesapeake and Delaware Bays, the Sough Slough estuary (Oregon), and York River (Virginia). Similarly high correlation (R^2 = 0.92) was observed between the $I_{Chla/R}{}^g$ magnitudes and the HPLC Chl *a* data for the same integrated data set. The WR normalization,

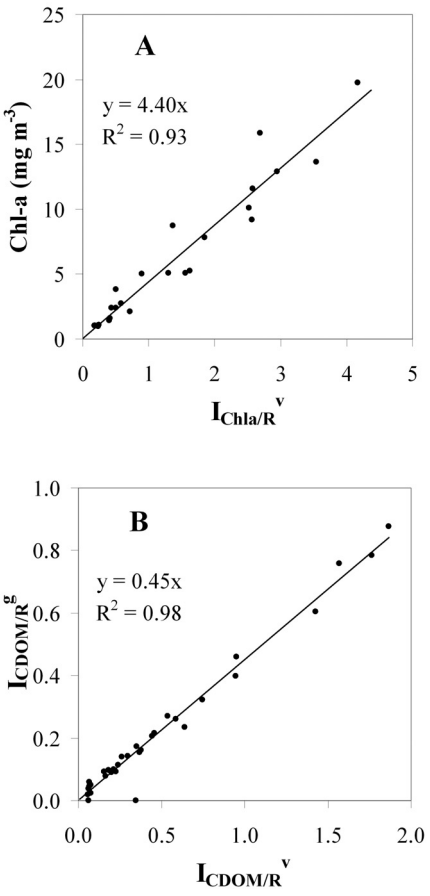

Fig. 7. (A): Correlation between the SDC retrievals of the $I_{Chla/R}{}^{v}$ fluorescence parameter and the HPLC measurements of total Chl *a* conducted in the Middle Atlantic Bight, Chesapeake and Delaware Bays, and in the Sough Slough estuary (Oregon) and York River (Virginia). (B): Correlation between the $I_{CDOM/R}{}^{v}$ and $I_{CDOM/R}{}^{g}$ parameters of CDOM fluorescence measured with 405 and 532 nm excitation, respectively, in the Delaware Bay and adjacent coastal and offshore areas of the Middle Atlantic Bight.

as well as the relatively short (<1cm) path of the excitation and emission light in the measurement cell, likely provided for the robustness of the correlation between Chl *a* fluorescence and concentration up to 20 mg m^{-3} despite the significant variability in turbidity (up to 10 NTU as measured in the York River) within the data set.

Assuming that the CDOM fluorescence stimulated at 405 and 532 nm originates from the same organic chromophores, comparison of the $I_{CDOM/R}{}^{v}$ and $I_{CDOM/R}{}^{g}$ magnitudes may provide a good overall test for the ALF SDC analysis. Indeed, the CDOM and WR emission bands are located in different portions of the LSE^{v} and LSE^{g} spectra and have different and variable patterns of spectral overlap with the emission bands of other water constituents (Figs. 5 and 6). In spectrally complex environments, the peak magnitudes of the CDOM and WR emission often constitute only a fraction of the LSE intensity at their peak locations (for example, see Figs. 5B, 5C, 5F, 6A, 6B, 6C, 6E, and 6F). Nonetheless, the correlation analysis yielded consistently high linear correlations between the $I_{CDOM/R}{}^{v}$ and $I_{CDOM/R}{}^{g}$ retrievals in various water types examined. For example, Fig. 7B displays their correlation for the combined data set measured in the Delaware Bay and adjacent coastal and offshore areas of the Middle Atlantic Bight.

To evaluate the ALF/SDC potential for assessment of the PBP-containing photosynthesizing organisms in the mixed phototrophic populations, we compared ALF SDC retrievals of the group-specific PE spectral indices with independent HPLC measurements of alloxanthin and zeaxanthin, the carotenoid biomarkers for the cryptophytes and cyanobacteria, respectively (Mackey et al. 1996). Fig. 8 displays the correlations for the water samples collected in the Southern California Bight in May 2007. High linear correlation, R^2 = 0.77, was found between the magnitudes of the $I_{PE3/R}{}^{g}$ fluorescence parameter and the alloxanthin concentration (Fig. 8A) despite its relatively low magnitudes. A similar linear correlation, R^2 = 0.78, was observed between the $I_{PE1/R}{}^{g}$ values and the zeaxanthin concentration (Fig. 8C). We interpret these data as a demonstration that the ALF/SDC retrievals provide potential for detection, discrimination and quantitative assessment of cryptophytes and cyanobacteria in natural aquatic environments.

Assuming the alloxanthin, zeaxanthin, and Chl *a* concentrations as proxies for biomass of cryptophytes, cyanobacteria, and total population of the photosynthesizing microorganisms, respectively, the alloxanthin/Chl *a* and zeaxanthin/Chl *a* ratios can be considered as first-order indices for assessment of relative abundance of cryptophytes and cyanobacteria in the mixed phototrophic populations. We evaluated the relationships between these pigment indexes and respective fluorescence parameters yielded by the SDC LSE analysis. For the data sets displayed in Figs.8A and 8C, the correlations between the $I_{PE3/Chla}$ vs. alloxanthin/Chl *a* ratio (Fig. 8B) and $I_{PE1/Chla}$ vs. zeaxanthin/Chl *a* ratio (Fig. 8D) were somewhat lower (R^2 = 0.63), which can be explained by the higher errors in the ratios vs. the absolute magnitudes of fluorescence and HPLC retrievals (Figs. 8A and 8C). The magnitudes of both pigment and fluorescence ratios were in the range of a few percent, which might also affect the correlations. Nonetheless, we consider the trends observed in Figs. 8B and 8D as a stimulus to further explore the potential of the ALF/SDC technique for structural analysis of the mixed algal populations.

Spectral correction of variable fluorescence—As described in Materials and Procedures, the real-time SDC LSE^{v} analysis yields the $I_{NC/Chla}$ parameter to assess the non-Chl *a* background emission in the area of Chl *a* fluorescence peak, B_{NC}. The latter is then subtracted from the PDP induction curve to retrieve spectrally corrected variable fluorescence (Eqs. 12-14). The ALF field spectral measurements have shown that the magnitudes of B_{NC} and relevant $I_{NC/Chla}$ parameters may exhibit significant variations in natural aquatic environments. For example, in surface oceanic waters the $I_{NC/Chla}$ magnitude may vary from a few percent (Fig. 5A) to 25 percent depending on the relationship

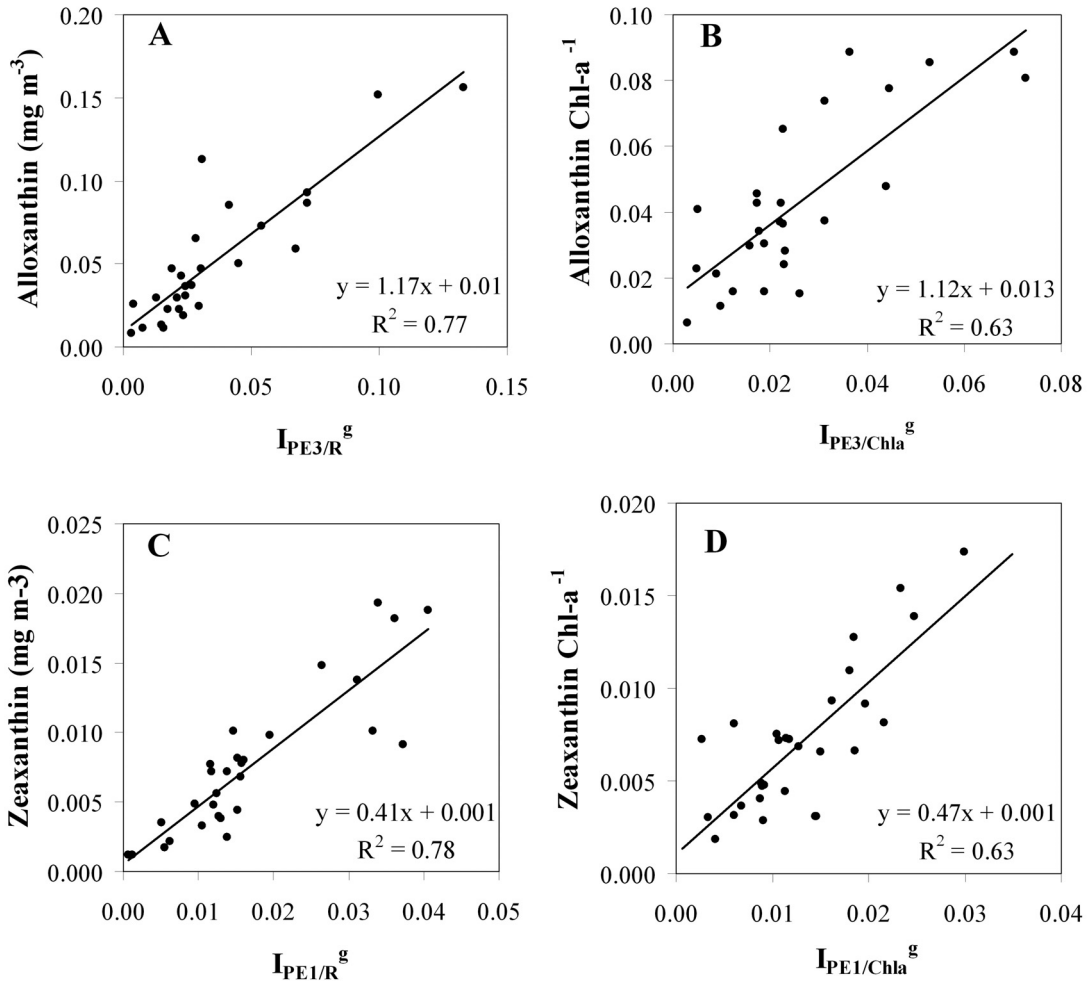

Fig. 8. Correlations between the group-specific PE spectral indices retrieved by the SDC LSE analysis and HPLC measurements of alloxanthin and zeaxanthin, the carotenoid biomarkers for the cryptophytes and cyanobacteria, respectively. The data demonstrate ALF potential for discrimination and quantitative assessment of the PE-containing photosynthesizing organisms in mixed populations.

between the CDOM and Chl *a* fluorescence intensity. The non-Chl *a* red fluorescence bands F_{R2} and/or F_{R3} also may provide a comparable to or greater than CDOM contribution in the spectral range of Chl *a* fluorescence peak (Figs. 5C and 5D, respectively). The $I_{NC/Chla}$ magnitude may reach 50%-100% in the CDOM-rich freshwater or estuarine environments (Fig. 5F) or at the bottom of euphotic layer (Fig. 5E). In the latter case, a decline in the Chl *a* fluorescence is typically accompanied by the increase in CDOM fluorescence and the broadband red emission of other non-Chl *a* constituents (for example, Fig. 5E and the vertical profiles of $I_{CDOM/R}{}^{v}$ and $I_{R3/R}{}^{v}$ in Fig. 11A discussed below). In extreme cases, the non-Chl *a* red background emission may significantly exceed the peak magnitudes of the Chl *a* and CDOM fluorescence (e.g., Fig. 5B).

The ALF spectral correction of variable fluorescence was designed to provide automatic accounting for the variable B_{NC} background in the analyzed water samples, thus yielding more accurate assessments of variable fluorescence in the spectrally complex aquatic environments. To illustrate the importance of the spectral correction, Fig. 9 displays the $I_{NC/Chla}$ magnitudes and the comparison of the F_v/F_m values calculated with and without the correction for the B_{NC} parameter for the water samples taken in the Delaware River between Trenton (New Jersey) and the river mouth adjacent to the Delaware Bay in June 2006. As evident from these data, up to 35% underestimation of the F_v/F_m magnitude might occur without the spectral correction due to the high CDOM content in the turbid waters (F_v/F_m = 0.29 vs. 0.45 at station 4 in the middle of the transect; the F_v/F_m values as high as 0.65 were observed here after the spectral correction during the phytoplankton spring bloom in April 2008). The ALF spectral correction of variable fluorescence is automatically and routinely conducted in real time during the discreet sample analyses and underway shipboard measurements (for example, see the spectrally corrected F_v/F_m transect data in Fig. 10). It needs no filtration or other treatment of the sample, and can be implemented in various instrument configurations and settings

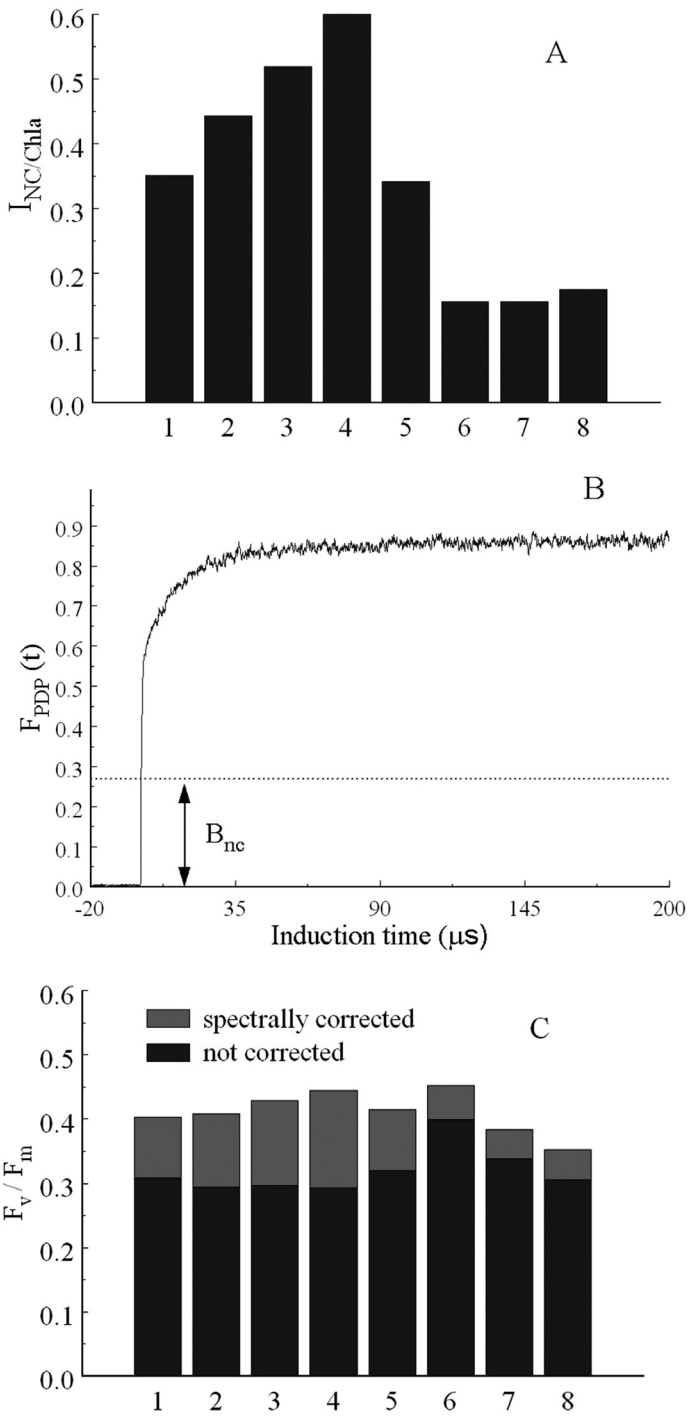

Fig. 9. Spectral correction of variable fluorescence for non-Chl *a* background emission in the area of Chl *a* fluorescence peak, B_{NC}. (A): The SDC retrievals of $I_{NC/Chla}$, the ratio of the non-Chl *a* background emission to the actual intensity of Chl *a* fluorescence in the LSE^v spectrum, at eight stations in the Delaware River, June 2006. (B): Fluorescence induction, $F_{PDP}(t)$, measured by the ALF instrument at station 4. The B_{NC} = 0.27 was calculated for $I_{NC/Chla}$ = 0.6 using Eq. 13 (see the LSE^v of this sample in Fig. 5F). (C): B_{NC} subtraction from the measured induction curves, $F_{PDP}(t)$, has yielded up to 35% increase in variable fluorescence, F_v/F_m, versus the retrievals without spectral correction.

potentially capable of the broadband SDC spectral measurements, including the in situ and airborne sensors of variable fluorescence (e.g., Chekalyuk et al. 2000).

ALF transect measurements—A significant amount of the ALF underway flow-through measurements onboard research ships and small vessels was acquired during the instrument deployments in diverse water types in 2005-2008. To illustrate the analytical capabilities of the ALF/SDC underway analysis, we present an example of the transect measurements conducted on 21 June 2006 in the coastal zone of the Middle-Atlantic Bight adjacent to the Delaware Bay. Distributions of the SDC-retrieved fluorescent parameters are displayed in Fig. 10B; the major transect features are marked with numbers to relate them with their spatial locations respectively numbered on the map in Fig. 10A. An arrow in panel B marks a technical break in the data acquisition occurred between points 6 and 7. The $I_{Chla/R}{}^v$ values have been converted into the units of Chl *a* concentration (right vertical axis in Fig. 10B) based on the linear correlation displayed in Fig. 7A. Magnitudes of the other ALF variables, including the spectrally corrected variable fluorescence, F_v/F_m, can be assessed using the left axis of the plot. The F_v/F_m values varied in the 0.3-0.4 range along the entire transect, thus showing a somewhat depressed physiological status of the phytoplankton population. Seven Chl *a* peaks, ranging from 5 to 13 mg m^{-3}, were detected along the transect indicating costal mesoscale variability in phytoplankton biomass. As evident from the $I_{CDOM/R}{}^v$ distribution, the CDOM spatial variability followed closely the Chl *a* spatial patterns suggesting a biological origin of CDOM in the surveyed area. The PBP-containing cryptophytes, indexed by the $I_{PE3/R}{}^g$ fluorescence parameter, showed quite patchy and somewhat distinct spatial patterns, compared to those of Chl *a*, reaching the highest concentration in the DB mouth (points 1, 2, 4 and 8, Fig.10A). By contrast, the high PUB/PEB PE-containing cyanobacteria indexed by the $I_{PE1/R}{}^g$ fluorescence parameter had their highest concentration in the coastal zone at point 5, with several smaller sub-peaks around points 0, 1, 2, and 8. The low PUB/PEB PE-containing cyanobacteria, characterized by the $I_{PE2/R}{}^g$ distribution showed spatial patterns well correlated with Chl *a*; they were most abundant in the Delaware Bay mouth (points 7-8), but also showed patchy structures in the adjacent section of the transect (points 0-2, 3-4, and 6).

Along with the characterization of pigment biomass, the ALF/SDC analysis has revealed significant structural variability in the mixed population of phytoplankton and cyanobacteria in the surveyed area. The cryptophytes were not detected along the initial, offshore portion of the transect and represented a relatively small fraction of the phototrophic community in the coastal zone of the Middle Atlantic Bight. This was indicated by the magnitudes of the $I_{PE3/Chla}$ parameter that were below 0.05 along the transect everywhere except the sharp peak around point 1, where they reached 0.1 (not displayed in Fig. 10B). A similar range of the $I_{PE3/Chla}$ variability was observed in the Southern California Bight and corresponded

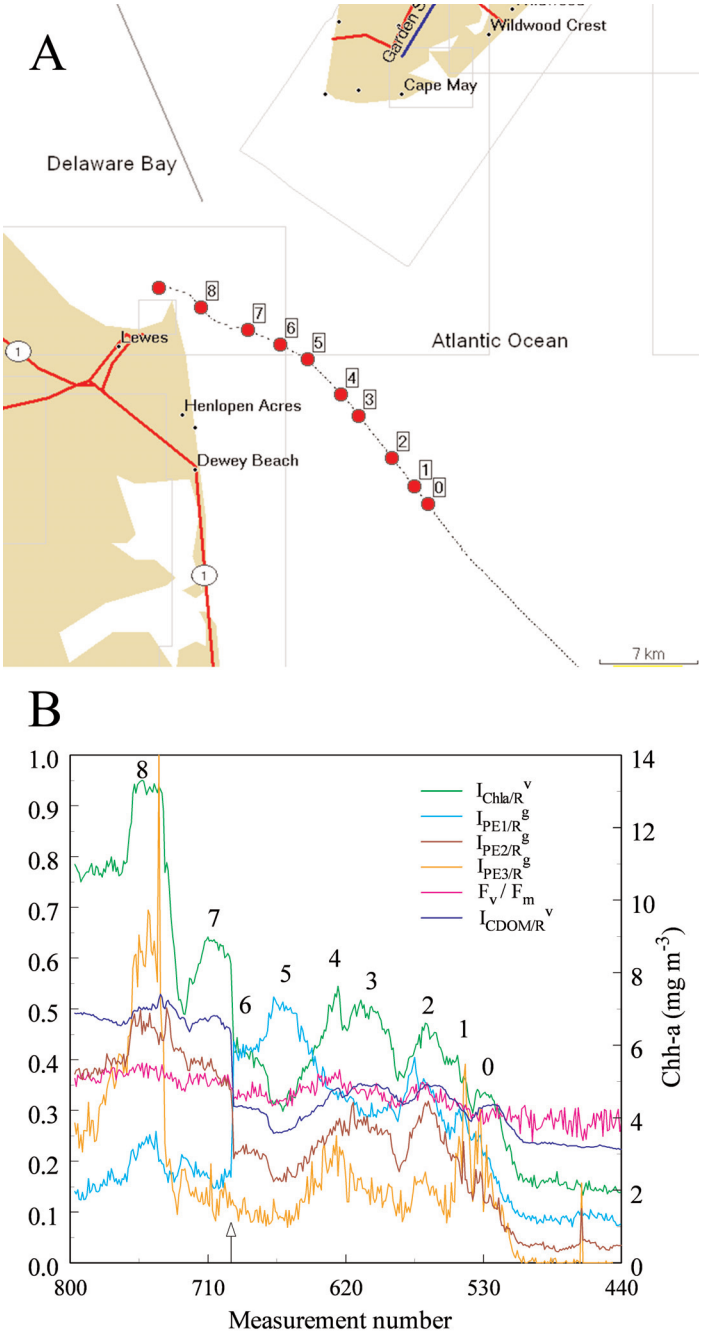

Fig. 10. An example of the shipboard underway ALF measurements in the coastal zone of the Middle-Atlantic Bight adjacent to the Delaware Bay, 21 June 2006. The major features of the transect distributions retrieved by SDC LSE analysis are marked in panel B with numbers to relate with their spatial locations respectively numbered on the map in panel A. The $I_{Chla/R}{}^{v}$ values have been converted into the units of Chl *a* concentration (right axis in panel B) using the correlation displayed in Fig. 7A. The spatial patterns indicate significant variability in pigments, CDOM, and phytoplankton structure in the surveyed area (see discussion in the text).

to the alloxanthin/Chl *a* ratio below 0.1 (Fig. 8B). By contrast, the high PUB/PEB PE-containing cyanobacteria were more abundant in the population along the offshore and initial coastal portions of the transect as indexed by the $I_{PE1/Chla}$ magnitudes that reached 0.16 at point 5, one order of magnitude above the highest $I_{PE1/Chla}$ values observed in the Southern California Bight (Fig. 8D). In the Delaware Bay mouth (points 7-8), their fraction exhibited a very sharp decline with the $I_{PE1/Chla}$ values below 0.03. Within the cyanobacterial group, their high PUB/PEB PE spectral type was overwhelmingly dominant in the offshore waters and around point 5 as indicated by $I_{PE1/PE2}$ retrievals that varied here in the range of 2 to 3.5.

Vertical distributions of fluorescence constituents—Although the ALF/SDC suite was primarily developed for shipboard underway characterization of aquatic constituents in the surface waters, it can also provide useful complementary information via laboratory and field analyses of discrete water samples. Two examples of the vertical distributions of the fluorescent constituents, compiled using the ALF analysis of the dark-adapted water samples collected at various depths in the offshore and coastal oceanic waters, are presented in Fig. 11. The upper horizontal scale in the plots displays Chl *a* concentrations based on the $I_{Chla/R}{}^{v}$ regionally-analyzed correlation with the HPLC pigment data.

In the offshore waters of the California current (Fig. 11A), biomass of phototropic phytoplankton and Type1, high PUB/PEB cyanobacteria (indexed by the $I_{Chla/R}{}^{v}$ and $I_{PE1/R}{}^{g}$ magnitudes, respectively) had almost identical vertical distributions, showing their gradual buildup with depth in the upper 50 m followed by a sharp increase to their maximum magnitudes at 75 m and the fast decline to less than a few percent of their maxima at 150 m. The ALF assessments of the Chl *a* concentration were 0.18 and 0.48 μg/L, in the samples from 2 and 75 m, respectively. No PE3 fluorescence was detected at this location indicating absence of cryptophytes in the phytoplankton population, as was consistently observed in the offshore waters of the California current. The spectrally corrected variable fluorescence, F_v/F_m, gradually increased from 0.19 at 5 m depth to 0.3 at 95 m below the Chl *a* maximum; no photosynthetically active Chl *a* was detected by the SDC analysis at 150 m. The low F_v/F_m magnitudes indicated a generally depressed photo-physiological status of phytoplankton despite the relatively high Chl *a* concentration in the Chl *a* peak. The CDOM content indexed by the $I_{CDOM/R}{}^{v}$ parameter showed no significant change in the upper 50 m of the water column, a 2-fold gradual increase between 50 and 150 m, and a slower rise with depths between 150 and 500 m (ALF measurements of the 500 m sample are not displayed). The $I_{R1/R}{}^{v}$, $I_{R2/R}{}^{v}$, and $I_{R3/R}{}^{v}$ magnitudes, which quantify the broadband red fluorescence typically observed below the Chl *a* maximum (for example, see Fig. 5E), exhibited a significant increase at 50-150 m, consistent with the above hypothesis that it may be due to fluorescence of a degrading pigment photosystem. Contrary to the CDOM emission, further gradual decline in

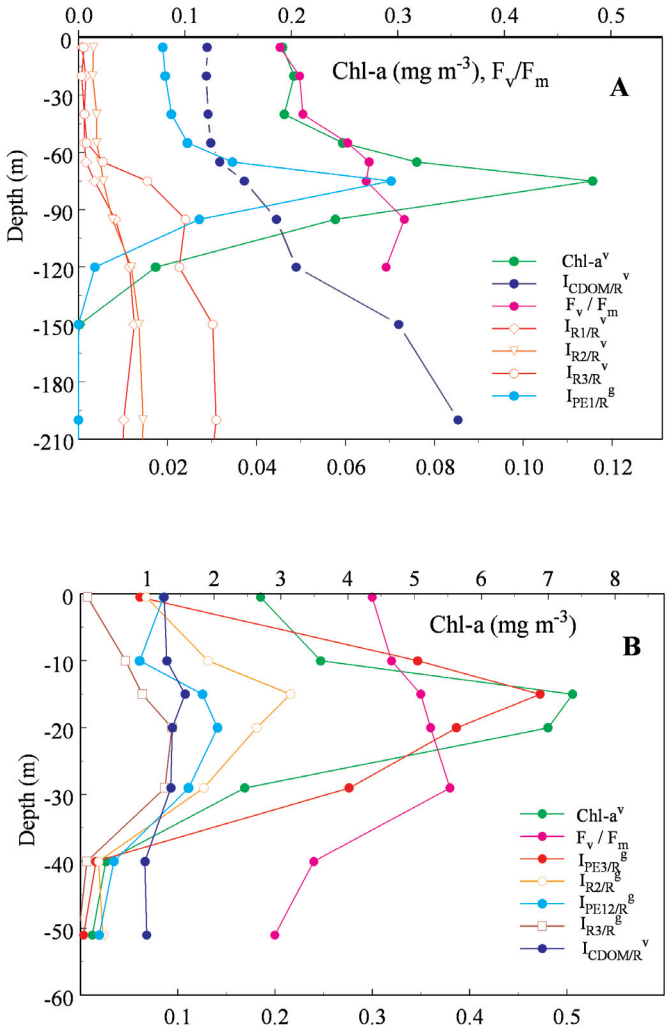

Fig. 11. Examples of vertical profiles of fluorescence parameters in the euphotic layer retrieved from the ALF sample measurements in (A) offshore waters of California current and (B) near Point Conception in coastal zone of the Southern California Bight. The upper horizontal axes provide scales for Chl *a* concentration (A, B) and F_v/F_m (A) calculated from the ALF measurements.

the $I_{R1/R}{}^v$, $I_{R2/R}{}^v$, and $I_{R3/R}{}^v$ magnitudes was typically observed below the bottom of the euphotic layer (i.e., below 150-200 m in Fig. 11A).

In the coastal zone of the South California Bight near Point Conception, most SDC-retrieved fluorescent parameters reached their peak magnitudes at much shallower depths, 15-20 m (see Fig. 11B). Significantly higher surface and peak magnitudes of Chl *a* concentration, 2.74 and 7.18 mg/L, respectively, were detected. The intense F_{PE3} fluorescence, with the peak value of the cryptophyte-specific parameter $I_{PE3/R}{}^g$ as high as 0.47, was observed in the water samples thus indicating significant cryptophyte abundance at this location (confirmed by the HPLC analysis). Though the $I_{PE12/R}{}^g$ magnitudes indexing the cyanobacterial biomass were somewhat higher compared to the offshore cast samples, the low, ~0.03, $I_{PE12/Chla}$ values indicated a relatively small fraction of cyanobacteria in the coastal phototrophic population. The vertical distribution of variable fluorescence, F_v/F_m, showed a slow gradual rise with depth from 0.3 at the surface to 0.38 at 30 m followed by decline to 0.2 at 51 m. Similar to the offshore profile, the F_v/F_m peak was located somewhat deeper than the maximum of the pigment biomass (30 vs. 15 m, respectively). By contrast to the offshore measurements, the CDOM fluorescence profile, $I_{CDOM/R}{}^v$, was more uniform. It reached its peak in the pigment maximum at 15 m followed by a gradual 30% decline between 15 and 50 m. The green-induced red fluorescence, peaking at 644 nm and indexed by the $I_{R2/R}{}^g$ magnitudes, showed the vertical profile correlated well with the cryptophyte-specific PE fluorescence indexed by $I_{PE3/R}{}^g$. The vertical profile of another green-induced red emission fluorescence, peaking at 662 nm and indexed by $I_{R3/R}{}^g$ parameter, was, rather, correlated with the vertical distribution of the cyanobacterial high PUB/PEB PE fluorescence, $I_{PE12/R}{}^g$. The observed patterns suggest that the red emission consistently detected in the LSE^g signatures around 644 and 662 nm may be associated in these PBP-rich coastal waters with in vivo fluorescence of phycocyanin and allophycocyanin, respectively.

Discussion

The described ALF/SDC analytical suite was designed to provide new tools for characterization of the fluorescent constituents in natural waters and bioenvironmental monitoring. The ALF is a compact, easily transportable and deployable flow-through instrument for high-resolution shipboard underway measurements over a range of spatial and temporal scales as well as discrete sample analyses. The ALF technology takes advantage of selective dual-wavelength laser excitation and broadband LSE spectral detection combined with spectrally corrected measurements of variable fluorescence. The SDC LSE analysis allows retrievals of the overlapped emission bands of aquatic constituents and more accurate photo-physiological assessments of photosynthesizing organisms. The ALF measurements provide real-time information about intensity and spectral variability in Chl *a*, phycoerythrin, and CDOM fluorescence. This novel approach may lead to improved assessments of pigment biomass and CDOM content, indication of structural changes in the phytoplankton community, and quantitative assessment of the PBP-containing phytoplankton and cyanobacteria.

The ALF dual-wavelength violet/green laser excitation provides for assessment of the key fluorescent constituents, including CDOM, Chl *a*, and PE pigments. The 405 nm excitation is efficient in assaying of CDOM (Fig. 5) and variable fluorescence, but cannot be used for PE analysis because of low PE absorption in the violet spectral range. The 532 nm excitation provides for efficient PE fluorescence stimulation, but yields generally more complex LSE^g signatures (see Fig. 6 for

examples). As shown by the initial field deployments, the ALF dual-wavelength excitation also extends the concentration range of Chl *a* assessments. For example, the $I_{Chla/R}{}^{v}$ parameter measured with 405 nm excitation has yielded quite reasonable assessments of Chl *a* concentration during measurements of the dinoflagellate blooms in the York River (>50 mg m^{-3}) and in Monterey Bay (>100 mg m^{-3}), where the accuracy of the $I_{Chla/R}{}^{g}$ retrievals was somewhat compromised.

The use of lasers for emission excitation also provides certain advantages over the broadband light emitting diodes or flash lamps often utilized in the field fluorometers. Indeed, as evident from the sample LSE spectra in Figs. 5 and 6, WR scattering is an important and often dominant LSE spectral component. With the narrow-band laser stimulation, it has the characteristic, relatively narrow spectral band, which allows its reliable SDC detection and discrimination in the overlapped LSE spectral patterns. The broadband excitation would result in respective broadening of the Raman spectral band (Desiderio et al. 1997), thus significantly complicating its discrimination from the constituent fluorescence. Normalization of the constituent fluorescence to WR scattering accounts for the highly variable optical properties of natural waters (Klyshko and Fadeev 1978; Hoge and Swift 1981) and creates units that can be directly compared with the data acquired by various shipboard and airborne laser fluorosensors.

As shown by the ALF field measurements, the LSE signatures measured in the diverse water types represent complex and highly variable patterns formed by the overlapped spectral bands of fluorescent aquatic constituents (see Figs. 5 and 6). Because of the spectral overlap, the spectral intensity at the wavelength of the constituent emission in most cases overestimates the actual intensity of the constituent emission. The overestimation is particularly significant in the estuarine, bay and fresh waters known to be spectrally complex (e.g., see Figs. 5B, 5C, 5F, 6C and 6E), but it may occur as well in the oceanic waters (for example, Figs. 5D, 5E, 6F). Accounting for the spectral overlap is particularly important for the correct fluorescence assessment of PE pigments (see Figs. 6B, 6C, 6E, 6F and the relevant discussion above) and water Raman scattering (Figs. 5B, 5C, 5F, 6B-F). The SDC LSE analysis allows for accurate retrievals of the constituent bands, thus providing for improved qualitative and quantitative constituent assessment. Incorporation of the broadband hyperspectral LSE SDC analysis in the shipboard (Klyshko and Fadeev 1978; Babichenko et al. 1993; Chekalyuk et al. 1995) and airborne (Hoge and Swift 1981; Hoge et al. 1998; Chekalyuk et al. 2000) laser remote sensing and in situ laser measurements (Cowles et al. 1989, 1993; Desiderio et al. 1993) may further improve our observational capabilities and provide new important information about natural aquatic environments over a range of spatial and temporal scales.

Another aspect of the spectral complexity of natural waters concerns the accuracy of photo-physiological assessment of photosynthesizing organisms via measurements of variable fluorescence. As revealed by the ALF field spectral measurements in various water types, the background non-Chl *a* emission produced by CDOM and other constituents in the spectral area of Chl *a* fluorescence may vary in a range of several to hundred percent of the Chl *a* fluorescence intensity. Not accounting for the non-Chl *a* fluorescence background may result in significant, up to 35%-50%, underestimation of the magnitude of variable fluorescence (see Fig. 9 and comments in *Assessment*). The spectrally corrected photo-physiological assessment of variable fluorescence is another distinct feature of the ALF measurement and analytical protocols that provides for improved characterization of the natural aquatic environments.

Comments and recommendations

At the initial stage of the ALF development reported in this communication, the research was focused on (i) designing the robust compact laser spectrofluorometer capable of routine broadband LSE/PDP measurements in the field, (ii) acquiring a set of field observations representing diverse water types, and (iii) the thorough analysis of the laboratory and field ALF measurements to develop the new analytical algorithms. A significant amount of work still needs to be done to fully implement the analytical potential of the ALF technique. In particular, most of the constituent fluorescence parameters yielded by the SDC algorithms need to be converted into the commonly accepted units (e.g., constituent concentrations) via a series of laboratory and field calibrations. Though the correlations between the Chl *a* fluorescence retrievals and independent assessments of Chl *a* concentration look reasonably good, the available field data sets need to be analyzed to verify the robustness of the correlation in the extended concentration range and the regional/seasonal dependence of the correlation parameters that may affect the accuracy of the fluorescence retrievals. At the short time scale, the diel variability in the pigment fluorescence yield (e.g., Falkowski and Kiefer 1985; Dandonneau and Neveux 1997) needs to be accounted for to further improve assessments of Chl *a* and PBP concentrations from the shipboard underway flow-through measurements. The ALF measurements of variable fluorescence may provide important feedback to the LSE spectral analysis of Chl *a* and PBP fluorescence to account for the photo-physiological variability in the pigment fluorescence yields. The field-based observations of spectral variability in Chl *a* fluorescence also need better understanding, which may provide new means for assaying phytoplankton physiology and functional groups. The detected in the field red emission peaks at 625, 644, and 662 nm need to be identified and interpreted to provide additional information about pertinent complex bio-geochemical processes in the natural aquatic environments. Extension of the ALF measurements and the SDC algorithms into the near ultraviolet and infrared spectral range may yield valuable information about other water constituents, such as spectrally-distinct forms of CDOM and bacteriochlorophyll.

Finally, the ALF methods and analytical protocols, which have been tested and employed in the flow-through instrument, can be implemented in variety of instrument configurations and settings, including in situ and airborne laser fluorosensors, to improve our capacity for oceanographic observations and bioenvironmental monitoring.

References

Babichenko, S., L. Poryvkina, V. Arikese, S. Kaitala, and H. Kuosa. 1993. Remote sensing of phytoplankton using laser-induced fluorescence. Remote Sens. Environ. 45:43-50.

Beutler, M., K. H. Wiltshire, B. Meyer, C. Moldaenke, C. Luring, M. Meyerhofer, U.-P. Hansen, and H. Dau. 2002. A fluorometric method for the differentiation of algal populations in vivo and in situ. Photosynth. Res. 72:39-53.

Chekalyuk A. M., A. A. Demidov, V. V. Fadeev, and M. Y. Gorbunov. 1995. Lidar monitoring of phytoplankton and organic matter in the inner seas of Europe-EARSeL Adv. Remote Sens. 3:131-139.

———, F. E. Hoge, C. W. Wright, and R. N. Swift. 2000. Airborne test of LIDAR pump-and-probe technique for measurements of phytoplankton photochemical parameters. Photosynth. Res. 66:45-56.

Cowles, T. J., J. N. Moum, R. A. Desiderio, and S. M. Angel. 1989. In situ monitoring of ocean chlorophyll via laser-induced fluorescence backscattering through an optical fiber. Appl. Optics 28:595-600.

———, R. A. Desiderio, and S. Neuer. 1993. In situ characterization of phytoplankton from vertical profiles of fluorescence emission spectra. Mar. Biol. 115:217-222.

Cullen, J. J., and R. F. Davis. 2003. The blank can make a big difference in oceanographic measurements. Limnol. Oceanogr. Bull. 12:29-35.

Dandonneau, Y., and J. Neveux. 1997. Diel variations of in vivo fluorescence in the eastern equatorial Pacific: an unvarying pattern. Deep Sea Res. II 44:1869-1880.

Del Castillo C. E., F. Gilbes, P. G. Coble, and F. E. Muller-Karger. 2000. On the dispersal of riverine colored dissolved organic matter over the west Florida shelf. Limnol. Oceanogr. 45:1425-1432.

Desiderio, R. A., T. J. Cowles, J. N. Moum, and M. Myrick. 1993. Microstructure profiles of laser induced chlorophyll fluorescence spectra: Evaluation of backscatter and forward scatter fiber optic sensors. J. Atmos. Oceanic Technol. 10:209-224.

———, C. Moore, C. Lantz, and T. J. Cowles. 1997. Multiple excitation fluorometer for in situ oceanographic applications. Appl. Optics 36:1289-1296.

Exton, R. J., W. M. Houghton, W. Esaias, R. C. Harriss, F. H. Farmer, and H. H. White. 1983*a*. Laboratory analysis of techniques for remote sensing of estuarine parameters using laser excitation. Appl. Optics 22:54-64.

———, ———, ———, R. C. Haas, and D. Hayward. 1983*b*. Spectral differences and temporal stability of phycoerythrin fluorescence in estuarine and coastal waters due to the domination of labile cryptophytes and stabile cyanibacteria. Limnol. Oceanogr. 28:1225-1231.

Falkowski, P., and D. A. Kiefer. 1985. Chlorophyll *a* fluorescence in phytoplankton: relationship to photosynthesis and biomass. J. Plankt. Res. 7:715-731.

———, and Z. Kolber. 1995. Variations in chlorophyll fluorescence yields in phytoplankton in the world oceans. Aust. J. Plant Physiol. 22:341-355.

Fuchs, E., R. C. Zimmerman, and J. S. Jaffe. 2002. The effect of elevated levels of phaeophytin in natural waters on variable fluorescence measured from phytoplankton. J. Plankton Res. 24:1221–1229.

Govindjee. 1995. Sixty-three years since Kautsky chlorophyll *a* fluorescence. Aust. J. Plant Physiol. 22:131-160.

Heocha, C. O. 1965. Biliproteins of algae. Ann. Rev. Plant Physiol. 16:415-434.

Hilton J., E. Rigg, and G. Jaworski. 1989. Algal identification using in vivo fluorescence spectra. J. Plankton Res. 11:65-74.

Hoge, F. E., and R. N. Swift. 1981. Airborne simultaneous spectroscopic detection of laser-induced water Raman backscatter and fluorescence from chlorophyll *a* and other naturally occurring pigments. Appl. Optics 20:3197-3205.

———, C. W. Wright, T. M. Kana, R. N. Swift, and J. K. Yungel. 1998. Spatial variability of oceanic phycoerythrin spectral types derived from airborne laser-induced fluorescence emissions. Appl. Optics 37:4744-4749.

Hudson N., A. Baker, and D. Reynolds. 2007. Fluorescence analysis of dissolved organic matter in natural, waste and polluted waters – a review. River Res. Appl. 23:631-649.

Iglesias-Prieto, R., N. S. Govind, and R. K. Trench. 1991. Apoprotein composition and spectroscopic characterization of the water-soluble peridinin—Chlorophyll *a*—Proteins from three symbiotic dinoflagellates. Proc. Roy. Soc. Lond. B 246:275-283.

Juhl, A. 2005. Growth rates and elemental composition of Alexandrium Monilatum, a red-tide dinoflagellate. Harmful Algae 4:287-295.

Juhl, A. R., and M. C. Murrell. 2005. Interactions between nutirnets, phytoplankton growth, and microzooplankton grazing in a Gulf of Mexico estuary. Aquat. Microb. Ecol. 38:147-156.

Klyshko, D. N., and V. V. Fadeev. 1978. Remote determination of concentration of impurities in water by the laser spectroscopy method with calibration by Raman scattering. Sov. Phys. Dokl. 23:55-59.

Kolber Z., O. Prazil, and P. G. Falkowski. 1998. Measurements of variable chlorophyll fluorescence using fast repetition rate techniques: defining methodology and experimental protocols. Biochim. Biophys. Acta. 1367:88-106.

Laney, S. R., and R. M. Letelier. 2008. Artifacts in measurements of chlorophyll fluorescence transients, with specific application to fast repetition rate fluorometry. Limnol.

Oceanogr. Methods 6:40-50.

Lantoine, F., and J. Neveux. 1997. Spatial and seasonal variations in abundance and spectral characteristics of phycoerythrins in the tropical northeastern Atlantic Ocean. Deep-Sea Res. I 44:223-246.

Lazar, D. 1999. Chlorophyll *a* fluorescence induction. Biochim. Biophys. Acta. 1412:1-28.

Mackey, M. D., D. J. Mackey, H. W. Higgins, and S. W. Wright. 1996. CHEMTAX - a program for estimating class abundances from chemical markers: application to HPLC measurements of phytoplankton. Mar. Ecol. Progr. Ser. 144:265-283.

Mimuro M., N. Tamai, A. Murakami, M. Watanabe, M. Erata, M. M. Watanabe, M. Tokutomi, and I. Yamazaki. 1998. Multiple pathways of excitation energy flow in the photosynthetic pigment system of a cryptophyte, Cryptomonas sp. (CR-1). Phycol. Res. 46:155-164.

Nash, J. C. 1979. Compact numerical methods for computers: Linear algebra and function minimization. Wiley.

Neveux, J., F. Lantoine, D. Vaulot, and D. Marie. 1999. Phycoerythrins in the southern tropical and equatorial Pacific Ocean: Evidence for new cyanobacterial types. 1999. J. Geophys. Res. 104:3311-3321.

———, M. M. B. Tenorio, C. Dupouy, and T. A. Villareal. 2006. Spectral diversity of phycoerythrins and diazotroph abundance in tropical waters. 2006. Limnol. Oceanogr. 51:1689-1698.

Oldham, P. B., and I. M.Warner. 1987. Analysis of natural phytoplankton populations by pattern- recognition of two-dimensional fluorescence-spectra. Spectrosc. Lett. 20:391-413.

Olson, R. J., A. M. Chekalyuk, and H. M. Sosik. 1996. Phytoplankton photosynthetic characteristics from fluorescence induction assays of individual cells. Limnol. Oceanogr. 41:1253-1263.

———, H. M. Sosik, and A. M. Chekalyuk. 1999. Photosynthetic characteristics of marine phytoplankton from pump-during-probe fluorometry of individual cells at sea. Cytometry 37:1-13.

———, and others. 2000. Effects of iron enrichment on phytoplankton in the Southern Ocean during late summer: active fluorescence and flow cytometric analyses. Deep-Sea Res. II 47:3181-3200.

Ong, L. J., and A. N. Glazer. 1991. Phycoerythrins of marine unicellular cyanobacteria. J. Biol. Chem. 266:9515-9527.

Poryvkina, L., S. Babichenko, S. Kaitala, H. Kuosa, and A. Shalapjonok. 1994. Spectral fluorescence signatures in the characterization of phytoplankton community composition. J. Plankton Res. 16:1315-1327.

Schreiber, U., C. Neubauer, and U. Schliwa. 1993. PAM fluorometer based on medium-frequency pulsed Xe-flash measuring light: A highly sensitive new tool in basic and applied photosynthesis research. Photosynth. Res. 36:65-72.

Sciandra, A., L. Lazzara, H. Claustre, and M. Babin. 2000. Responses of growth rate, pigment composition and optical properties of *Cryptomonas* sp. to light and nitrogen stresses. Mar. Ecol-Prog. Ser. 201:107-120.

Seppala, J., and M. Balode. 1998. The use of spectral fluorescence methods to detect changes in the phytoplankton community. Hydrobiologia 363:207-217.

Van der Weij-De Wit, C. D., and others. 2006. How energy funnels from the phycoerythrin antenna complex to Photosystem I and Photosystem II in cryptophyte *Rhodomonas* CS24 cells. J. Phys. Chem. B. 110:25066-25073.

Wirick, C. 1994. Exchange of phytoplankton across the continental shelf-slope boundary of the Middle Atlantic Bight during spring 1988. Deep-Sea Res. 41:391–410.

Wood, A. M., P. K. Horan, K. Muirhead, D. Phinney, C. M. Yentsch, and J. B. Waterbury. 1985. Discrimination between types of pigments in marine *Synechococcus* spp. By scanning spectroscopy, epifluorescence microscopy, and flowcytometry. Limnol. Oceanogr. 30:1303-1315.

———, D. A. Phinney, and C. M. Yentsch. 1998. Water column transparency and the distribution of spectrally distinct forms of phycoerythrin-containing organisms. Mar. Ecol-Prog. Ser. 162:25-31.

Wright, C. W., F. E. Hoge, R. N. Swift, J. K. Yungel, and C. R. Schirtzinger. 2001. Next generation NASA airborne oceanographic lidar system. Appl. Opt. 40:336-342.

Yentsch, C. S, and C. M. Yentsch. 1979. Fluorescence spectral signatures - characterization of phytoplankton populations by the use of excitation and emission spectra. J. Mar. Res. 37:471-483.

———, and D. A. Phinney. 1984. Fluorescence spectral signatures for studies of marine- phytoplankton. Adv. Chem. Ser. 209:259-274.

——— and ———. 1985. Spectral fluorescence - an ataxonomic tool for studying the structure of phytoplankton populations. J. Plankton Res. 7:617-632.

Submitted 28 February 2008
Revised 3 September 2008
Accepted 1 October 2008

Limnol. Oceanogr.: Methods 6, 2008
© 2008, by the American Society of Limnology and Oceanography, Inc.

Advanced laser fluorometry of natural aquatic environments

Alexander Chekalyuk[1]* *and Mark Hafez*[2]
[1]Lamont Doherty Earth Observatory of Columbia University, Marine Biology 4a, 61 Rt. 9W, Palisades, NY 10964
[2]EG&G Services Inc., NASA Wallops Flight Facility, Bldg. N159, Wallops Island, VA

Appendix A:

Table 2. Parameters of the Pearson's IV function(s) for the analytical approximation of the SDC components of the constituent emission bands observed in natural waters*

Spectral component	Emission Band	λ_{max}, nm	a_o	a_1	a_2	a_3	a_4
E_{CDOM}^{v}	CDOM fluorescence	505	1	505.2	87.7	2.22	–2.85
E_R^{v}	Water Raman scattering:	471	0.025	422.3	1.49	0.413	–0.988
	1660, 2200, and 3440 cm^{-1}		0.016	434.8	1.35	0.789	0.540
			0.008	444.2	1.01	4.20	–76.5
			0.619	466.7	5.11	2.68	–0.539
			0.759	471.2	6.60	3.72	0.019
			0.190	474.8	3.62	4.54	12.3
			0.019	484.5	3.27	3.60	–23.3
E_{CDOM}^{g}	CDOM fluorescence	583	1	583.1	3.28	1.66	–71.6
E_R^{g}	Water Raman scattering:	651	0.042	583.3	2.24	0.852	0.650
	1660, 2200, and 3440 cm^{-1}		0.016	599.2	5.47	0.724	–0.710
			0.457	641.9	7.84	2.33	–0.291
			0.817	650.5	12.0	3.67	1.39
			0.169	657.9	2.87	3.35	19.6
			0.017	672.7	16.6	14.0	83.9
E_{R1}	Red emission 1	625	1	625.1	12.1	1.59	–3.11
E_{R2}	Red emission 2	644	1	644.0	17.2	1.80	–2.63
E_{R3}	Red emission 3	662	1	661.9	23.0	1.62	–1.65
E_{Ch1}	Chl-a fluorescence 1	673	1	673.4	13.7	2.95	–0.616
E_{Ch2}	Chl-a fluorescence 2	679	1	678.5	12.8	1.86	–0.444
E_{Ch3}	Chl-a fluorescence 3	692	1	692.1	16.1	2.23	–2.37
E_{PE1}	PE fluorescence 1	565	0.985	565.4	58.1	12.3	–16.9
			0.233	610.9	35.3	1.85	–2.49
E_{PE2}	PE fluorescence 2	578	0.954	577.9	14.1	1.14	–0.78
			0.163	613.8	70.3	8.17	7.74
E_{PE3}	PE fluorescence 3	590	1.000	589.8	21.0	1.56	–1.40
			0.056	617.1	14.6	3.57	–1.59
			0.063	628.1	18.1	4.67	0.487
E_E^{g}	Elastic scattering	532	1	543.9	0.913	1.01	–15.7
E_E^{v}	Elastic scattering, approximated with $y = a_0 \exp(-a_1\lambda)$	405	6.85e30	0.168			

*E_E^{v} is approximated with $y = a_0 \exp(-a_1\lambda)$. The superscripts "v" and "g" indicate excitation at 405 and 532 nm, respectively. If several lines of coefficients are listed, the emission band is presented as a sum of the Pearson's functions calculated with the listed coefficients.